Ray Tracing Simulation of an Electron Detector

Andreas Eriksson

Degree project for Bachelor of Science in Physics
15 hec

Department of Physics
University of Gothenburg

Faculty of Science

UNIVERSITY OF GOTHENBURG

Ray Tracing Simulation of an Electron Detector

Andreas Eriksson*

Abstract

In this thesis, a construction of an electron detector which is a part of an apparatus used for photo detachment experiments, is presented. The electron transmission through the detector device of the original construction is compared to the transmission in a modified model. The original and modified models are simulated and examined in the simulation software SIMION 8.0 that can visualize the device geometries and the trajectories of electron beams. In addition, as a part from the original construction, a simulation of a ninety degree energy analyzer is included in the setup, used for selecting different beam energies and allowing a beam with a certain energy to go through the device. As a final version of the detector two energy analyzers and two detector devices are combined into a new construction of the setup allowing detection of the electrons in two perpendicular directions simultaneously. The angular resolution with the double analyzers can then be measured without changing the polarization of the laser light.

*E-mail: guseandr83@student.gu.se

Contents

List of Figures

List of Tables

1 Introduction

In this section, some of the theoretical aspects relevant for experiments with negative ions, and the charged particle dynamics in the electron detector is introduced.

The apparatus is built for photodetachment experiments and by studying the angular resolution and energy of the electrons new information of the structure of the ions can be received. By performing the experiment in a collinear geometry, where an ion and a laser beam are merging into each other during an interval, a stronger signal to a detector makes it possible for carrying out experiments [1].

The outer electron shell in an atom, and especially the outermost electrons, gives information about the structure and dynamics of the electron system of a negative ion [2].

By determine, from theory and experiments, the binding energy of the outermost electrons from the electron affinity (EA) for an atom A

$$EA(A) = E_{tot}(A) - E_{tot}(A^-),$$

where E_{tot} is the total energy of the atom A and the negative ion A^-, one can determine whether the negative ion is stable (EA>0) or unstable (EA<0).

The photodetachment transition is a process where a negative ion A^- is interacting with photons γ and transforming into a neutral atom A and a photoelectron e^- with photo energy $\varepsilon_{if\gamma}$. For the transition from initial (i) to final state (f) the process can be written as

$$A^-(i) + \gamma \longrightarrow A(f) + e^-(\varepsilon_{if\gamma}) \tag{1}$$

From the photodetachment transition (1), the energy of the photoelectron is equal to

$$\varepsilon_{if\gamma} = E_\gamma - (E_f - E_i)$$

and determines the binding energy $(E_f - E_i)$, where E_i and E_f is the energy of the initial and final states in the transition, respectively and $E_\gamma = h\nu$ is the energy of the photons.

The threshold (THR) photon energy is determined from experiment by tuning narrow band laser by measuring the threshold frequency $\nu_{THR,if}$ and is equal to

$$E_{THR,if} = h\nu_{THR,if} = E_f - E_i$$

where h is Planck's constant[3].

The emitted electrons in this process is simulated in the angular resolution detector and the energy analyzer further below. In section 4.1 a schematic picture of the detector device shows where this process is taking place in the ion beam apparatus. Besides binding energies, also mass and size of the negative ions can be determined in the apparatus and the angular resolution detector device.

The goal with this thesis is to present a design of a modified construction of an angular resolution detector that has a higher electron transmission rate from the collinear laser and ion beam to a channel electron multiplier. The new construction of the device is compared to the original construction regarding the transmission rates.

2 Numerical Methods

2.1 SIMION 8.0

SIMION 8.0 is an optics simulation program that models ion and electron optics [4]. Electrostatic electrodes and/or magnetic poles can be created as potential arrays in an ion optics workbench which is an imaginary three dimensional rectangular volume of space where the simulations are performed. The arrays are pixel displays with an electrostatic or magnetic value.

Devices and instruments can be modeled in the workbench allowing the user to visualize and rotate the model in any space direction and cut out one or many cross sections for examining the trajectories of flying ions/electrons. The charged particles can be viewed as dots or lines evolving in the model when flying through it and data can be measured, recorded and saved into a text file for further analysis.

2.2 Electrostatics

The solution of the Laplace equation gives the E-field which is proportional to the force $\vec{F}$ that determines the trajectory of a charged particle flying in the field. A derivation of the partial differential equation from electrostatics follows below from [5].

For the electrical source charges $q_1, q_2, q_3, ...$ and a test charge Q we can compute the force $\vec{F_1}$ between q_1, F_2 between q_2 and Q and so forth. The total force $\vec{F}$ is a superposition of $\vec{F_1}, \vec{F_2}, \vec{F_3}, ...$ and is equal to the sum

$$\vec{F} = \vec{F_1} + \vec{F_2} + \vec{F_3} + ...$$

From Coulomb's law we have the force between a source charge q and a test charge Q with separation $\vec{r} = (x, y, z)$

$$\vec{F} = \frac{1}{4\pi\epsilon_0}\frac{qQ}{r^2}\vec{r}$$

where $\epsilon_0 = 8.85 \cdot 10^{-12} C^2/N \cdot m^2$ is the permittivity of free space and $\vec{r}$ is the position vector. Dividing the force $\vec{F}$ by Q gives the electrical field $\vec{E}$

$$\vec{E} = \frac{\vec{F}}{Q} = \frac{1}{4\pi\epsilon_0}\frac{q}{r^2}\vec{r}$$

Integrating the electrical field E over some path connecting the points O and r with a minus sign in front of the line integral gives the electrical potential which is defined as the function

$$V(\vec{r}) \equiv -\int_O^r \vec{E} \cdot d\vec{l}$$

and taking the derivative on both sides we get the electrical field

$$\vec{E} = -\vec{\nabla}V$$

which says that the electrical field is the gradient of a scalar potential, i.e the slope of a smooth potential surface.

The force is equal to the gradient of the potential multiplied by the charge Q

$$\vec{F} = -Q(\vec{\nabla}V)$$

and the potential also obeys the superposition principle as for the force F. Dividing the superposition of the force by the charge Q gives the superposition of the electrical field

$$\vec{E} = \vec{E_1} + \vec{E_2} + \vec{E_3} + ...$$

and integrating the electrical field gives the total potential $\vec{V}$

$$\vec{V} = \vec{V_1} + \vec{V_2} + \vec{V_3} + ... \tag{2}$$

The superposition principle for the electrical potential is important to the simulated model in chapter 5.2 where several electrodes with various voltages are combined and forming a potential hill having a smooth surface.

From the scalar potential $\vec{E} = -\vec{\nabla}V$ we get from one of Maxwell's equations (Gauss law)

$$\vec{\nabla} \cdot \vec{E} = \frac{\rho}{\epsilon_0}$$

where ρ is the space charge. Substituting $\vec{E} = -\vec{\nabla}V$ in the equation above gives

$$\vec{\nabla} \cdot \vec{E} = \vec{\nabla} \cdot (-\vec{\nabla}V) = -\vec{\nabla}^2 V$$

this reduces to the Poisson's equation

$$\vec{\nabla}^2 V = -\frac{\rho}{\epsilon_0}$$

In regions with no space charge we have $\rho = 0$ and Poisson's equation reduces to **Laplace's equation**

$$\boxed{\vec{\nabla}^2 V = \frac{\partial^2 V}{\partial x^2} + \frac{\partial^2 V}{\partial y^2} + \frac{\partial^2 V}{\partial z^2} = 0} \tag{3}$$

The solution V(x,y) of the Laplace's equation in two dimensions at some point (x,y) in the xy-plane is a solution to the equation

$$\frac{\partial^2 V}{\partial x^2} + \frac{\partial^2 V}{\partial y^2} = 0$$

and can be viewed as the rubber sheet model illustrated in figure 1 where the height of the surface above the xy-plane at the point (x,y) is equal to z=V(x,y). The rubber sheet model can be imagined as a sheet spanned over a frame where a sink in the sheet represents a negative potential and a ball made of steel represents a positive ion that allocates itself to the lowest point when rolling over the surface of the sheet.

In the simulations we have electrons and positive potentials in the device and the rubber sheet model in our case is reversed as in figure 1.

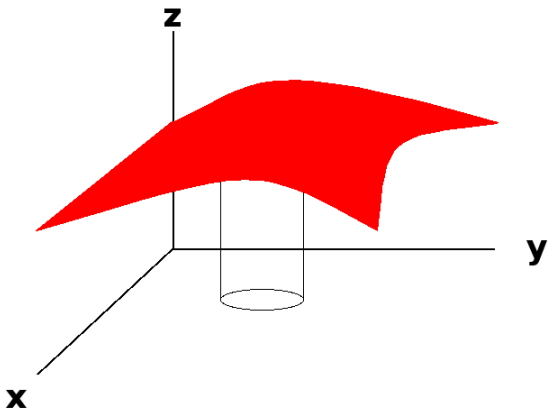

Figure 1: Laplace equation in two dimensions.

The value of V(x,y) is the average around the point (x,y) and is computed as the line integral around a circle centered at (x,y) and having radius R

$$V(x,y) = \frac{1}{2\pi R} \oint_{circle} V dl$$

This computation is called the method of relaxation where the solution V($\vec{r}$) of Laplace's in three dimensions is the average value around a point $\vec{r} = (x,y,z)$ over a spherical surface having radius R and is centered at $\vec{r}$

$$V(x,y,z) = \frac{1}{4\pi R^2} \oint_{sphere} V da$$

SIMION computes the relaxation method by using the nearest points in the workbench grid to obtain the new estimates [1] for each point [4]. In two dimensions the average of the four nearest points P_1, P_2, P_3 and P_4 around a point P_0 approximates a solution to Laplace's equation and in three dimensions adds a point P_5 on top and a point P_6 below P_0 according to the scheme

$$\begin{array}{ccc} & P_4 & \\ P_1 & P_0 & P_2 \\ & P_3 & \end{array} \qquad \begin{array}{l} \text{2D:} P_{0new} = (P_1 + P_2 + P_3 + P_4)/4 \\ \text{3D:} P_{0new} = (P_1 + P_2 + P_3 + P_4 + P_5 + P_6)/6, \end{array}$$

The fourth order Runge-Kutta numerical integration method is used in SIMION to calculate the trajectory of the ions in three dimensions. The Runge-Kutta integration in two dimensions evaluates integrals of the form [6]

$$y_{k+1} - y_k = \int_{t_k}^{t_{k+1}} f(t, y(t)) dt,$$

[1] The method of relaxation is an iterative technique where SIMION scans through the whole potential array that has a value applied and solving the Laplace's equation for each point.

for the time step t in the interval $t_k < t < t_{k+1}$, $k = 0, 1, 2, ...$ where the second argument of f, the solution $y(t)$, is unknown. The **Fourth order Runge-Kutta** numerical integration method is equal to the scheme [6]

$$y_{k+1} = y_k + \frac{h_k}{6}(k_1 + 2k_2 + 2k_3 + k_4), \tag{4}$$

where

$$\begin{aligned} k_1 &= f(t_k, y_k) \\ k_2 &= f(t_k + h_k/2, y_k + h_k k_1/2) \\ k_3 &= f(t_k + h_k/2, y_k + h_k k_2/2) \\ k_4 &= f(t_k + h_k, y_k + h_k k_3) \end{aligned}$$

with the step size $h_k = t_{k+1} - t_k$. Rearranging the terms in equation (4) gives the slope of the trajectory according to

$$\frac{y_{k+1} - y_k}{h_k} = \frac{1}{6}(k_1 + 2k_2 + 2k_3 + k_4)$$

The Runge-Kutta method is an iterative method for finding a solution to a differential equation. In other words, solving the ordinary differential equation of the form

$$\frac{dy}{dt} = f(t, y),\ y(0) = y_0$$

with the the first value $y_i = y_0 = y$, that is assumed to be known at time t_i, we can find the value of $y = y_{i+1}$ at time t_{i+1} [7].

3 Ion Optics and Electrode Geometries

3.1 Ion Optics

Electron and ion optics deal with the motion of electrons and ions in electrical and magnetic fields [8]. Electrostatic or magnetic forces changes the trajectories when the particles are traveling in a field created with help of various electrode or magnetic pole geometries.

A beam of ions or electrons in an electrostatic or a magnetic field is bent, accelerated or focused depending on various shapes geometries of the electrodes or the magnetic poles. Electrostatic and magnetostatic forces determines the trajectory of the ions or electrons flying through a field and in contrast to light optics, where the ray is refracted at interfaces of optical components, the beams in ion optics are changing direction gradually in a field. The ion beam is not visible, unlike a ray of light when smoke are blown over it, making a visualization program illustrating the path of the beam in an apparatus or a device crucial for examination of the trajectories. The relative energy (momentum) of an ion beam diminish when refracted in a section of electrodes (poles) and a strong initial energy at the ion source is therefore preferable, while the energy of a light beam remains approximately the same after reflection in a sequence of lenses [4].

The subsections below examine various geometries of deflectors, electrostatic and magnetic lenses and analyzers which are contained in the apparatus setup.

3.1.1 Einzel Lens

An Einzel lens is a cylindrical electrode focusing a beam around its central axis as shown in figure 2. A line with zero potential along the central axis of the cylinder is called an equipotential line where the ions or electrons have a straight trajectory when flying through the electrode. All trajectories deviating from the equipotential line are changing gradually and are focused to a point behind the cylinder. The light optics analogue of an Einzel lens is a positive lens.

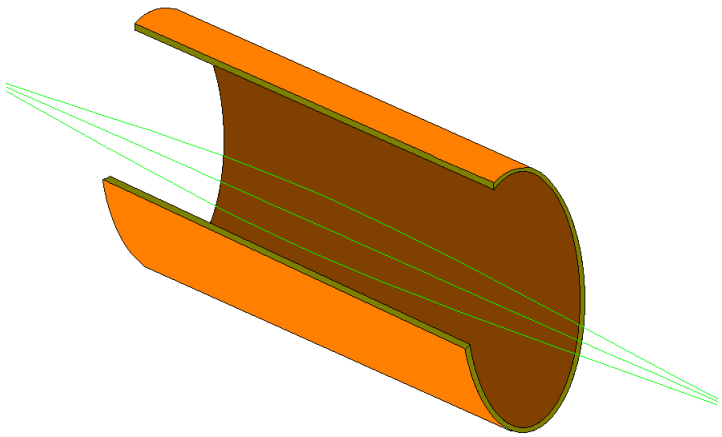

Figure 2: Einzel lens.

3.1.2 Quadrupole Deflector

A quadrupole deflector is made of two pairs of cylindrical electrodes with a positive and a negative voltage applied to each pair, respectively, as shown in figure 3. If the shape of the electrodes are given by the equation $x^2 + y^2 = r_0^2$, where r_0 is the distance from the center of the quadrupole to the electrodes, viewed from above, then the potential field in x and y directions are given by

$$E_x = -\frac{x}{r_0}\frac{2V_0}{r_0}$$

$$E_y = +\frac{y}{r_0}\frac{2V_0}{r_0}$$

where $\pm V_0$ are the voltages applied to the poles. An ion beam with a negative charge is deflected 90° in the quadrupole.

The apertures in the quadrupole are used in the apparatus to aim a laser beam through the deflector and merge with the ion beam where the photodetachment process can occur.

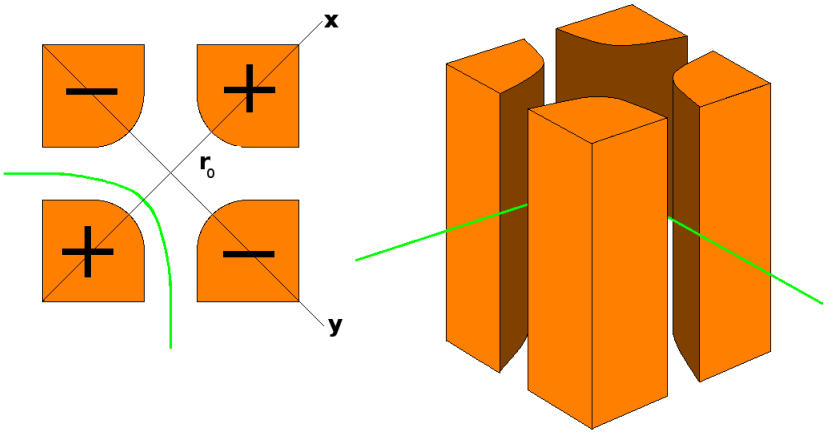

Figure 3: Quadrupole deflector.

3.1.3 Accelerator System

A simple acceleration system consisting of two electrodes with one aperture in each plate is shown from the side in figure 4.

For an ion beam having negative charge flying to the right in the figure, with the voltages $V_1 < V_2$ applied to the electrodes, the ions are gaining its kinetic energy $(1/2)mv^2 = -eV$ through the sequence of the electrodes. The electric field is assumed to be zero outside the system, a charged particle is accelerated in the region between the electrodes.

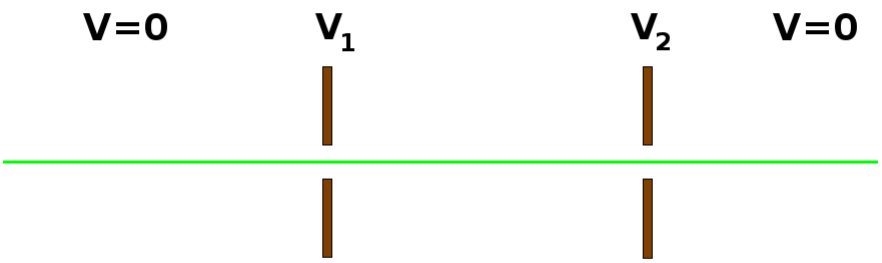

Figure 4: Accelerator system.

3.1.4 Deflection Plates and Energy Analyzer

Two rectangular electrodes with a positive and a negative voltage applied to each plate, respectively, is viewed from the side as shown in figure 5 a) and deflects two beams having different energies in one direction. The beam with the higher energy is less deflected in the gap between the electrodes; the negatively charged beam with trajectory closer to the central line between the plates has a higher initial kinetic energy compared to the beam whose whose trajectory is further away from the central line. Deflectors are used in the apparatus to adjust the direction of an ion beam to an aperture.

There is a scaling rule which is a relation between the initial beam energy and the voltage setting of the electrodes and is equal to the ratio

$$\frac{T}{e\Delta V} = constant$$

where T is the kinetic energy, e is the fundamental charge and ΔV is the difference in voltage setting of the electrodes. The ratio of increasing the initial beam energy and the voltages to the electrodes by an equal magnitude is constant and the deflection of the beam of ions or electrons remains unchanged.

The most simple construction of an energy analyzer is a pair of electrodes with opposite voltages applied as shown in 5 a) where charged particles are flying to the right. Such pair of electrodes with a slit placed to the right of the electrodes that can allow a beam with a certain initial energy to pass through is called an energy analyzer.

The electrodes in an analyzer can also be cylindrical as in figure 5 b). An analyzer with cylindrical electrodes is examined and simulated in section 5.4.

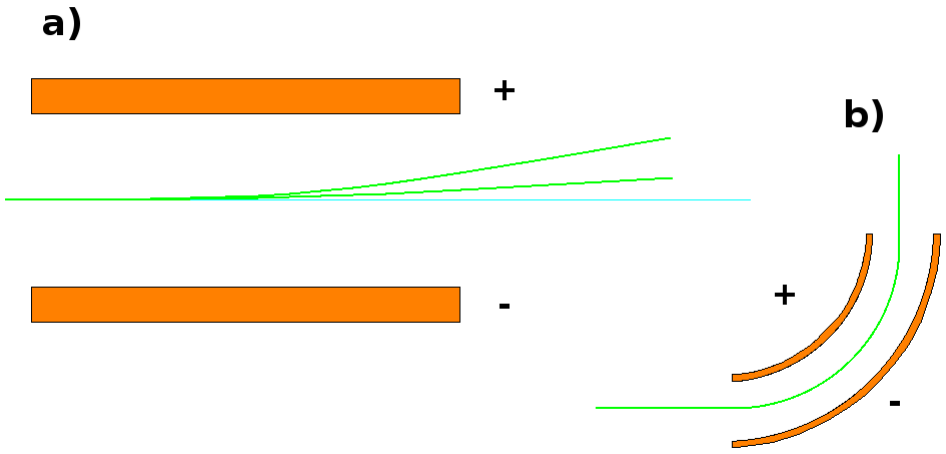

Figure 5: Energy analyzers.

3.1.5 Sector Magnet

A pair of magnets with north and south pole placed close to each other, with a pole gap, refracts a beam of charged particles in a circular motion in the magnetic field between the poles as shown in figure 6. The magnetic force $\vec{F}$ (Lorentz force) is equal to the cross product

$$\vec{F} = q(\vec{v} \times \vec{B})$$

where q is the charge, $\vec{v}$ is the velocity vector and $\vec{B}$ is the magnetic field vector. The force vector is perpendicular to the plane spanned by $\vec{v}$ and $\vec{B}$.

An ion beam with negative charge is deflected by the force $\vec{F}$ equal to $q(\vec{v} \times \vec{B})$ with the direction to the right relative to the beam direction and the magnetic poles as in figure 6. The radius of refraction is proportional to the mass m of the ions; r=(m/e)v/B, a sector magnet is due to this proportionality a mass analyzer.

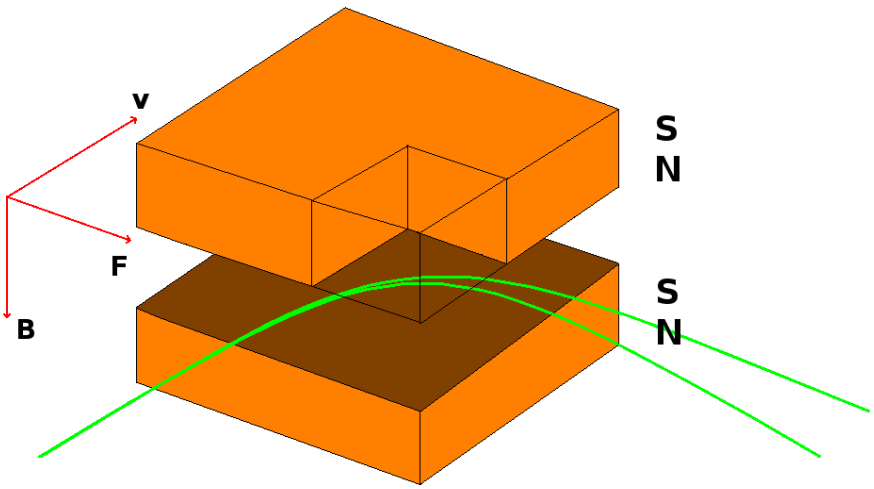

Figure 6: Sector magnet.

4 Experimental Setup

4.1 Ion Beam Apparatus

A schematic picture of the apparatus is shown in figure 7. The main parts of the apparatus is the ion source, a sector magnet where the ions are mass-analyzed, and the analyzing chamber in the last section. The angular resolution electron detector in the analyzing chamber is the device examined in more detail in subsection 4.2 and simulated in the subsections 5.1 and 5.2. The negative ion beam and a laser beam are merged in the analyzing chamber where photons are absorbed in the ions forming neutral atoms and free electrons.

A negative potential between the ion source and the grounded extractor, which has a 2 mm hole in its center, accelerates and sputter ions through a gas leaked into the vacuum chamber forming a beam of negative ions. The beam is directed towards two Einzel lenses (E1, E2) and four pairs of deflection plates (X1, Y1, X2, Y2). The two pair of deflector plates adjusts the beam in the horizontal (X) and vertical (Y) direction, relative the direction of the beam, into an aperture (A1). The beam passes through an aperture and entering the sector magnet with radius 0.5 m which bends the beam 90°.

From the sector magnet, the beam is going through a section with two Einzel lenses (E3, E4) and two pairs of deflection plates (X3, Y3, X4, Y4). The beam enters an aperture (A2) and is thereafter adjusted by a deflection plate (X5) in front of a quadrupole deflector (Q1) where the ion beam is merged with the laser beam over a 50 cm section that are ending at a second quadrupole deflector (Q2). An ion absorbs a photon where a neutral atom is created and emitting an electron that are detected.

The electron detector is placed between the two quadrupoles and from the beams, neutral atoms goes straight through the detector device and the second quadrupole, to the atom detector where they are hitting a plate made of glass where secondary emitted electrons are detected in a second channel electron multiplier (CEM2). The remaining negative ions in the beams deflects 90° and hitting a Faraday cup (F2) which is a metal plate connected to an Ampéremeter that measures the current from the ions. See [1] for more details.

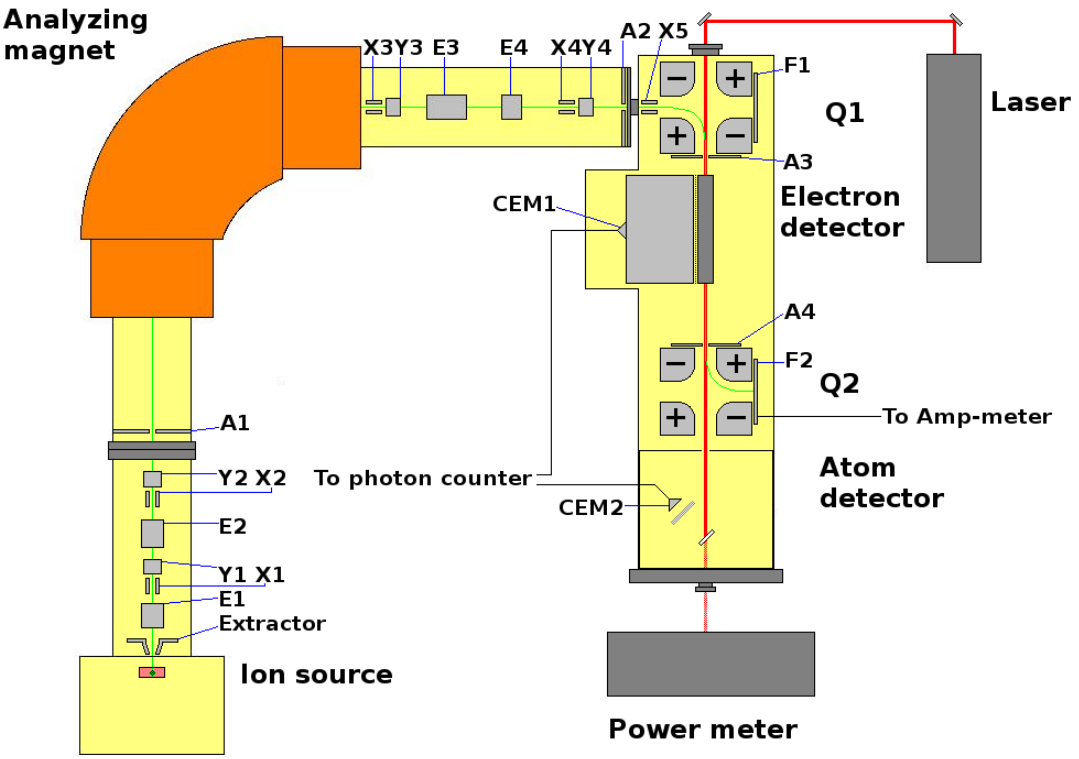

Figure 7: Schematic picture of the apparatus setup.

4.2 Angular Distribution Detector

The electron detector is used for measuring the angular distribution of the emitted electrons and is made of a 25 cm long graphite tube, whose central is axis along the path of the beams, with 67 holes drilled along one side. The cylindrical cavity of the tube has a diameter of 13 mm and the outer diameter of the tube is 32 mm. Each of the 67 holes on the side of the tube has a diameter of 2.5 mm. A channel electron multiplier (CEM) is mounted 10 cm in front of the tube facing the holes. A grounded metal box, with dimensions 25×10×10 cm, is placed between the graphite tube and the CEM and composes a framework for the detector device.

A channel electron multiplier device is made of an anode, a dynode and a cathode. The dynode is made of s semiconductor material, shaped as a curved cylindrical channel, where secondary emission of electrons occurs when an electron impinges its inner surface. The dynode is placed between the anode[2] and the cathode, with a high voltage applied to all the electrodes. Electrons are collected to the anode and thereafter accelerated to the dynode transferring some of its energy to the electrons in the dynode causing secondary electrons to be emitted and in turn accelerated inside the dynode releasing more electrons, with a repeating process, through the channel on to the cathode. A cascade of electrons is hitting the cathode and causing a current which can be amplified and analyzed. The gain is determined by the ratio of the length and the diameter of the dynode[9].

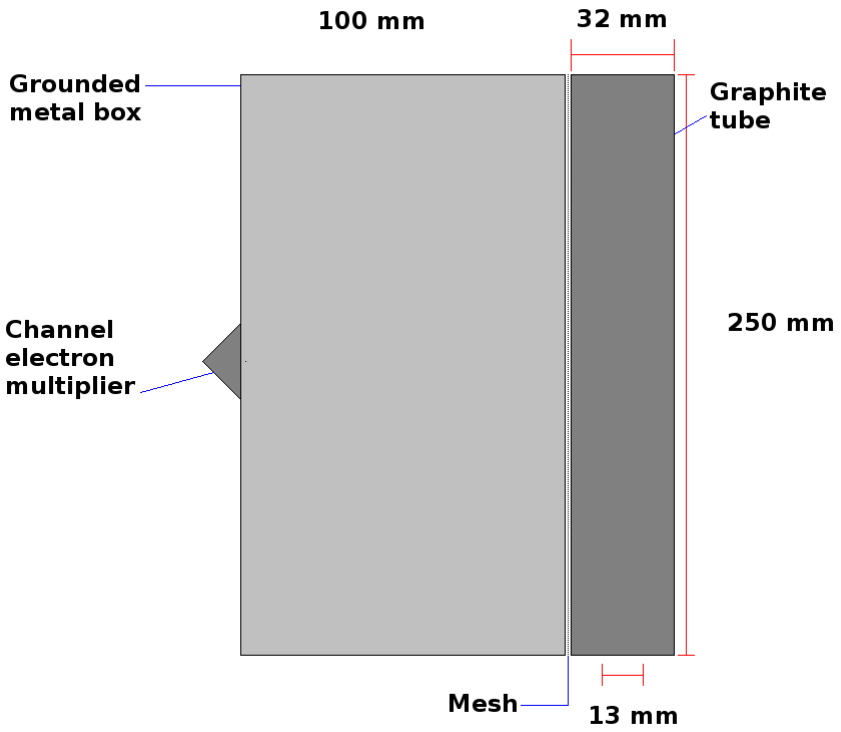

Figure 8: Schematic picture of the detector device.

[2]The CEM is viewed and modeled as a cone, which is the anode of the CEM, in the figures and in the simulations in section 5.1 and 5.2 but it is merely a simplification of the multiplier construction.

5 Simulations and Results

5.1 Simulations of the Original Construction

A laser and an ion beam, merged in the cavity of the tube in the angular resolution detector device where the photodetachment process is taking place, are forming neutral atoms and free electrons. The neutral atoms are transmitted through the tube and a quadrupole deflector for detection in an atom detector.

The electrons are emitted at random angle inside the cavity where a part of the emitted electrons are passing through the 67 holes on the side of the tube and are thereafter detected by the CEM mounted on the grounded box.

SIMION 8.0 has a limitation of 200 million points in the workbench and due to this limit different dimensions of the simulated model is not similar to the actual size of the device. The height of the box is lower than the real version and the dimensions of the box in the simulation seen in figure 9 is equal to 25×10×3.2 cm. The model is created from compiling a geometry file, which is a text file containing program code, from where SIMION creates electrodes and grounded geometries for the simulation model. Creating a model from a geometry file is preferred when the model has fine details, cavities, electrodes inside cavities, and complex three-dimensional constructions.

The user of the program can define the characteristics of the particles flying in the simulation such as quantity, mass, charge, beam energy, color, starting positions and distribution of the beam source. By defining the source position as a line sequence, with 67 duplicates where the first source is located at x=27.5 mm, y=16 mm, z=9.5 mm and and with a step size z=3.5 mm for the remaining consecutive sources, gives starting positions in the center of each hole on the side of the graphite tube.

By choosing a filled cone distribution with a half angle of 7.45 degrees one obtains maximum azimuthal-and elevation angle of the electron source with no loss in transmission due to interaction with the graphite tube. This dispersion angle gives a realistic source distribution of the electron beam inside the box when considering a large number of electrons flying from the apertures of the tube to the CEM.

The coordinates of the electrons in the x, y and z-directions flying in the device can be recorded and saved in a text file. SIMION has a recording parameter called "crossing plane x=" and initiating it to 118 mm defines an imaginary plane between the CEM and the box. Each electron entering the aperture of the box are recorded and saved as one line that are giving the position of where the electrons are crossing the imaginary plane.

With help of a text editor or a spreadsheet program, that can open a text file and enumerate the lines, the transmission rate of the electrons in the device can be calculated as being equal to the number of lines (for each electron hitting the CEM) divided by the total number of electrons (defined by the user) flying in the model:

$$\boxed{\text{Transmission rate} = \frac{\text{Number of electrons hitting the CEM}}{\text{Total number of electrons}}}$$

A cross section of the device with the trajectories of 400 electrons is shown in figure 10 where the setting of 200 volts to the CEM attracts a part of the electrons from the beam source. The red dots in front of the CEM shown in figure 10 and figure 11 are the coordinates where SIMION are recording the electrons crossing the imaginary plane.

The reduced height of the box does not decrease the transmission rate of the electrons since all the electrons are hitting the wall on the side of the box, where the CEM is mounted on, as shown in figure 12.

The trajectories of the electrons close to the CEM shown in figures 10 and 11 are curved towards the aperture of the box while the outermost trajectories are unaffected by the potential. The strength of the potential, with 200 volts applied, has a short range as shown in figure 13 comparing two contour lines of the potential added in the picture. The contour line inside the box of the potential 100 volts is limited in the interior of the cone and the contour line of the potential 1 volt has a more far-reaching span.

Setting the initial kinetic energy of the electrons in the beam to a fixed value of 1 eV and setting the CEM voltages from 200 volts, with a 200 volts increase in each consecutive step, up to 800 volts and calculating the transmission rate in each step gives an increasing sequence according to table 1.

The electron transmissions in table 1-3, gives the effectiveness of the CEM. The transmission through each hole in the side of the graphite tube is examined in more detail in section 5.3 by considering a partition of the tube with a beam source on the central axis in front of the aperture on the side.

Table 1: Channel electron multiplier settings and transmission rates.

CEM settings, Volts	Transmission, %
200	21-22
400	26-27
600	29-30
800	31-32

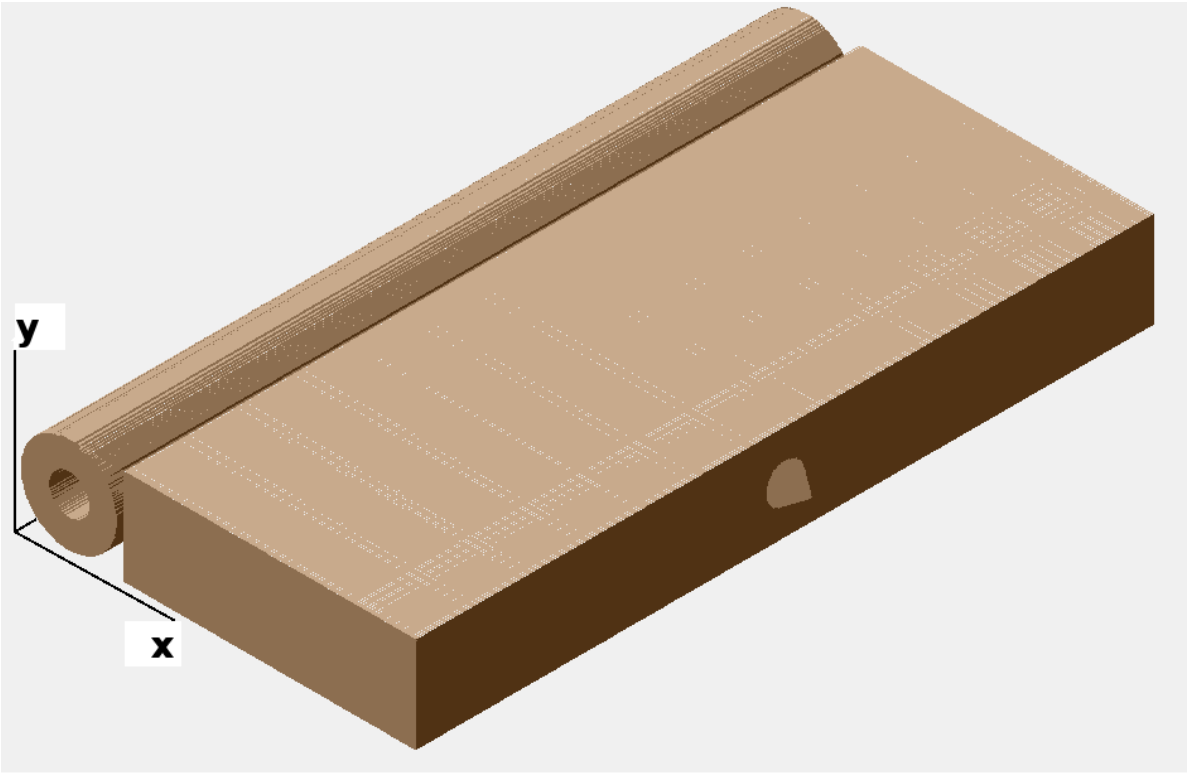

Figure 9: SIMION picture of the original construction of the detector device.

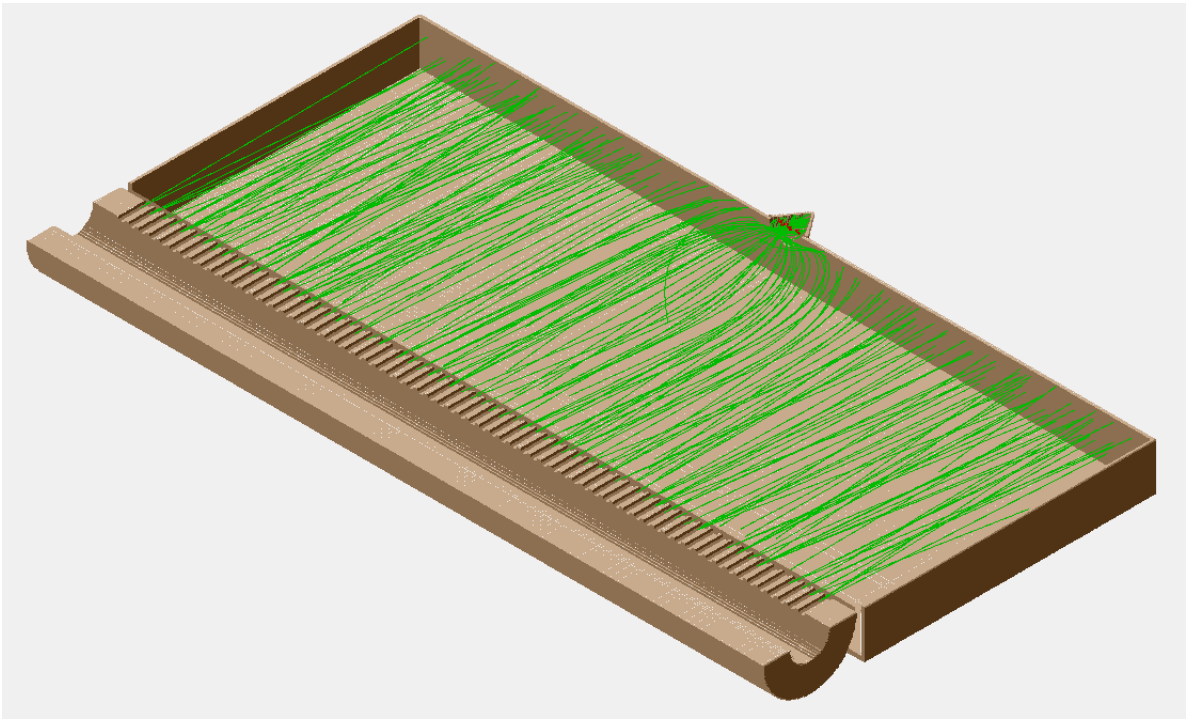

Figure 10: SIMION picture of the original construction of the detector device with the trajectories of 400 electrons.

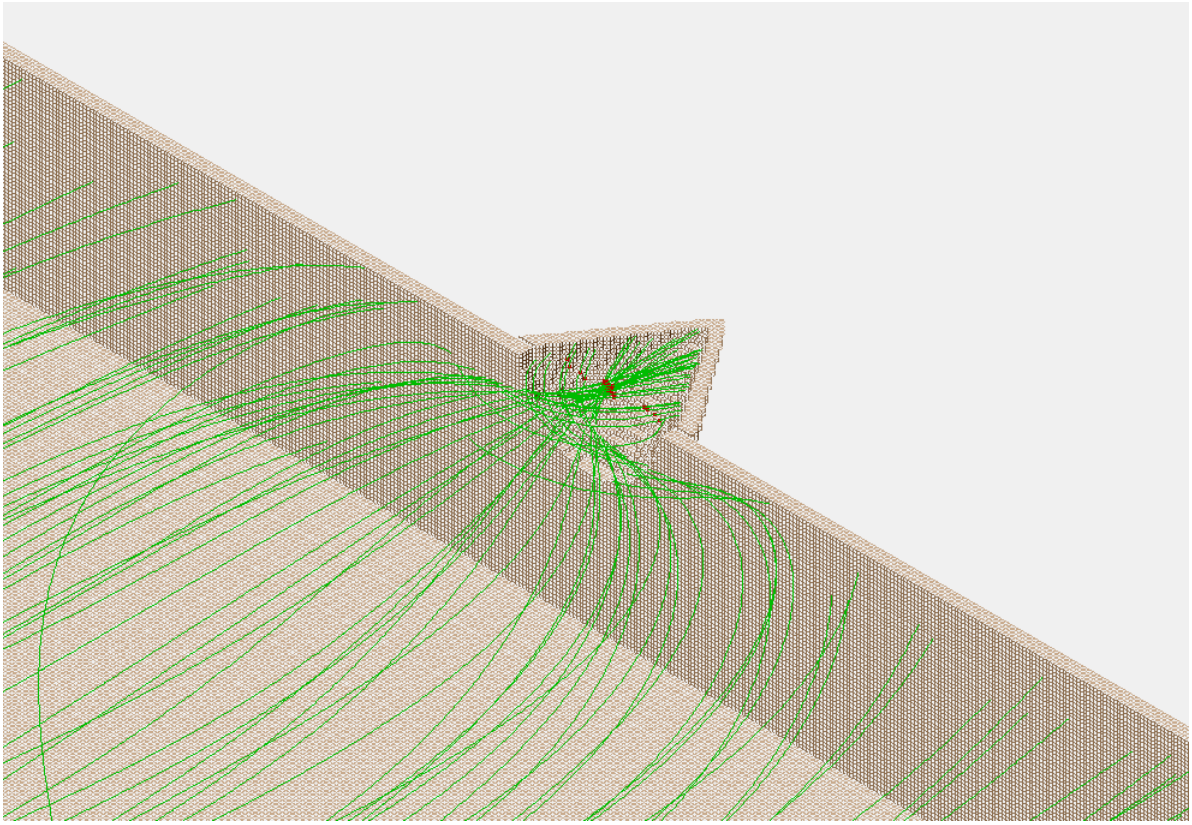

Figure 11: A magnified picture of the original construction zoomed in at the CEM.

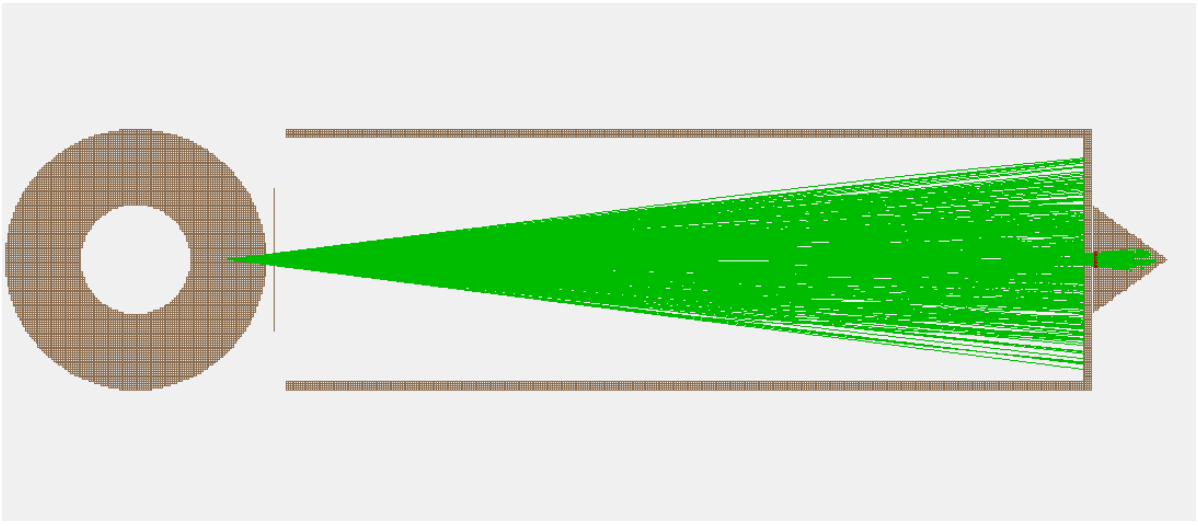

Figure 12: Cross section of the angular resolution detector with a beam of electrons viewed from the side.

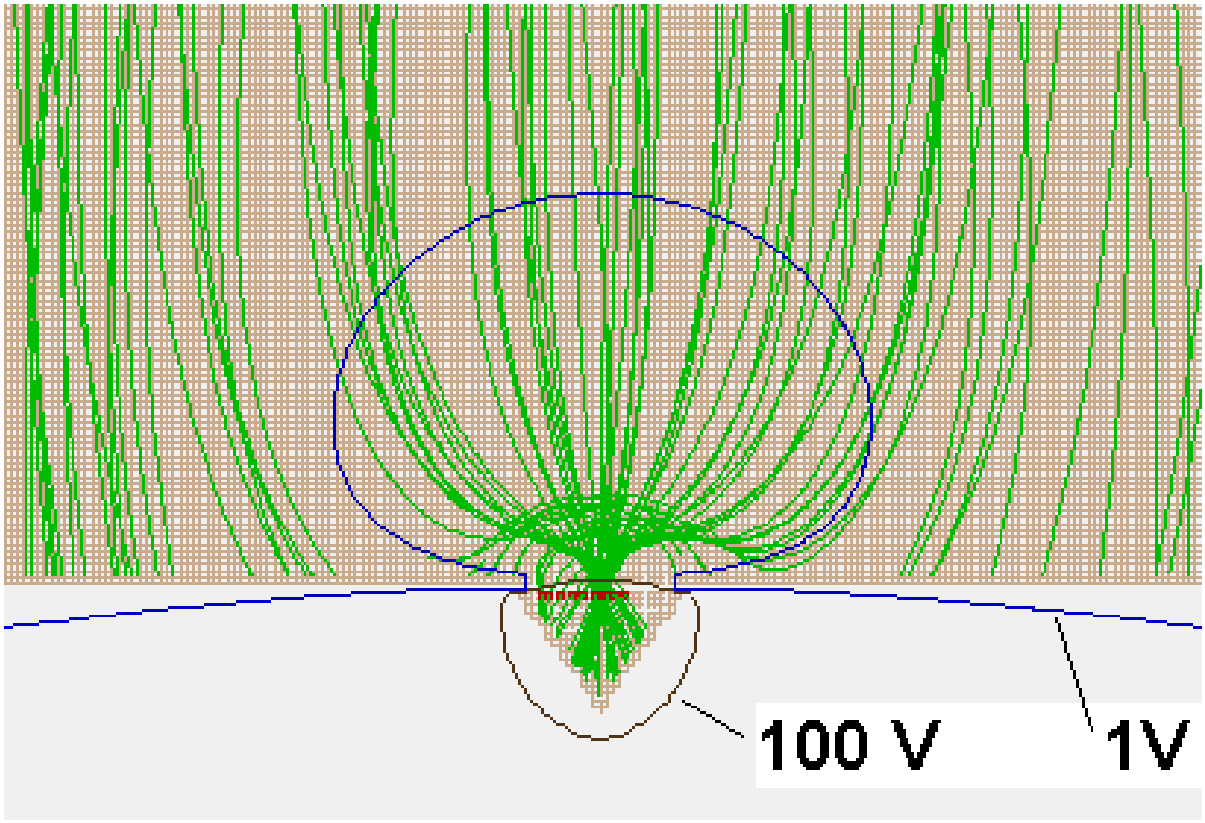

Figure 13: CEM with 200 volts applied and two contour lines of the potential field.

5.2 Simulations of the Modified Construction

Adding six pairs of electrodes on the top and bottom wall inside the box crates a potential hill where the negatively charged electrons are attracted to the highest point on the hill, in correspondence to a reversed rubber sheet model. The electrons from all apertures of the graphite tube are affected by the potential hill and the trajectories around the central electrode are bent inwards to the CEM.

The length of the box and the electrodes inside the box are extended by 5 cm and the increase makes the incidence angle of the flying electrons to the aperture of the CEM smaller and gives an increased electron transmission due to the more head-on trajectories. Further, the height is extended from 3.2 to 4.2 cm for giving more space between the electrodes.

The first pair of electrodes has the length 15 cm, width 19.5 mm, and thickness 1 mm and is placed right below and above the CEM perpendicular to the tube shown in figure 14. The consecutive pairs of electrodes are 45.5 mm wider than the previous pair where the sixth pair of electrodes are covering the entire surface of the top and bottom interior area of the box, as shown in figure 14 and figure 15.

The superposition of potentials, equation (2), implies an additive solution property of the Laplace equation (3). With six pairs of electrodes SIMION computes a solution to the Laplace equation for each electrode and adding each solution to the composite result (see especially appendix H.11 in [4]).

Let $P_{n1}, P_{n2}, P_{n3}, P_{n4}, P_{n5}, P_{n6}$, where n=any common array location, denote the solution of the electrode pair 1-6, then the composite potential P_n is computed as

$$P_n = P_{n1} + P_{n2} + P_{n3} + P_{n4} + P_{n5} + P_{n6} \tag{5}$$

Adjusting the voltages of the electrode pairs 1-6 to **4.7, 4.5, 3.6, 2.7, 1.5 and 1 volts**, respectively, and viewing the lower part of the device in PE-view in SIMION shows a potential hill for the superposition of the electrode voltages as in figure 16 and 17. The CEM is set to a moderate value of 7 volts in the figures to show the capturing of the electrons to the cone. The low contrast in voltages between the CEM and the electrode pairs makes it possible to visualize both the potential hill and the peak in the same picture.

The blue lines in the figures are the trajectories of thirty electrons flying in the device where the outermost electrons are affected by the slope of the hill ($\vec{\nabla}V$) that is proportional to the force ($\vec{F}$) that determines the curved trajectories of the electrons towards the CEM and the trajectories in front of the CEM are merely accelerated on a flat potential surface straight ahead through the device.

Flying electrons with the electrode settings according to above and with the range of the CEM voltages as in table 1 gives an approximate threefold increase of transmission rates according given in table 2. The extra electrodes inside the box affects all the trajectories of the electrons flying from the apertures as shown in figure 18.

Table 2: Channel electron multiplier settings and transmission rates for the modified device.

Multiplier settings, Volts	Transmission, %
200	60-61
400	75-76
600	83-84
800	86-87

The scaling rule $T/e\Delta V = constant$ does not apply to this configuration of electrodes. Increasing the beam energy from 1 eV to 10 eV while holding the CEM fixed at 200 volts and increasing all the electrode voltages tenfold results in a decrease of transmission. Using the scaling rule on beam energies 20 eV and 30 eV shows a declining trend in transmission as shown in table 3.

Viewing the simulation from above, in the xz-view, shows that the trajectories are curved too much towards the center where some electrons are getting out of range of the CEM and hitting the electrodes in front and besides the aperture of the box. Since the Coulomb force $\vec{F}$ is proportional to the slope of the potential hill $\vec{\nabla}V$ determines the deflection of the electron trajectories, the relation between the kinetic beam energy T and the gradient of the potential $\vec{\nabla}V$ does not give an invariant shape of the trajectories for various settings as in the case of a deflection plate, or analyzing, system where the gradient of the potential is constant over the plates.

Table 3: Beam energy, electrodes settings and transmission rates for the modified device.

Beam energy, eV	Electrode pairs no 1-6, V						Transmission, %
1	4.7	4.5	3.6	2.7	1.5	1	60-61
10	47	45	36	27	15	10	20-21
20	94	90	72	54	30	20	14-15
30	141	135	108	81	45	30	13-14

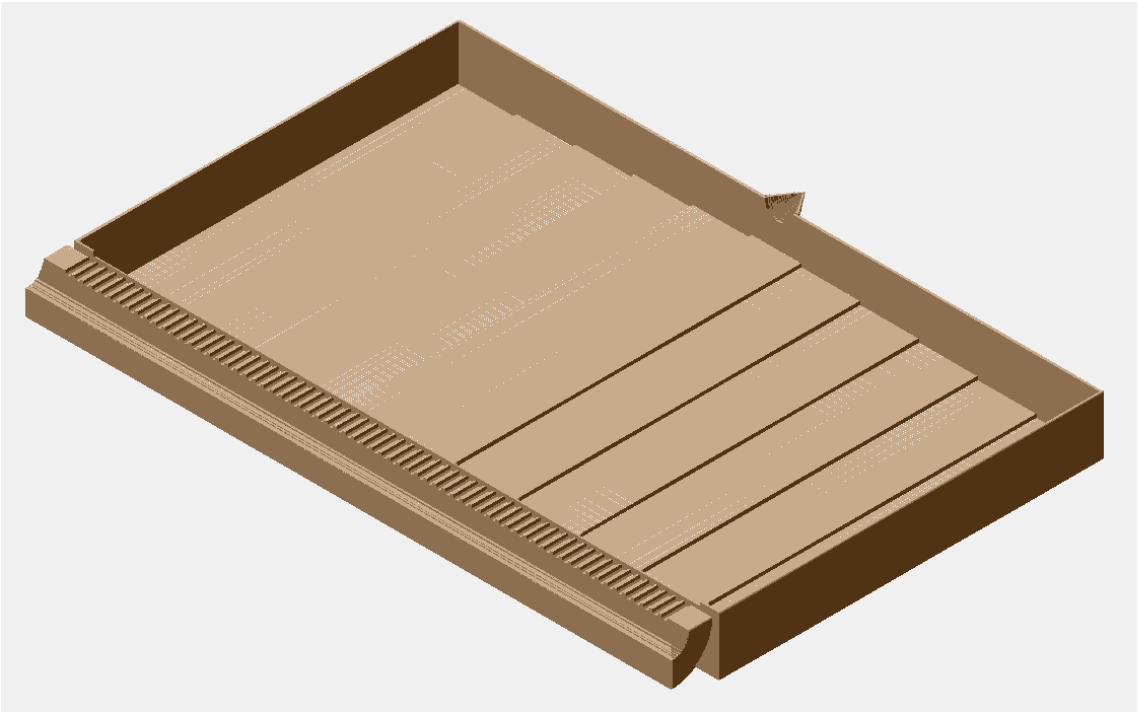

Figure 14: Cross section of the detector device with six pairs of electrodes inside the box.

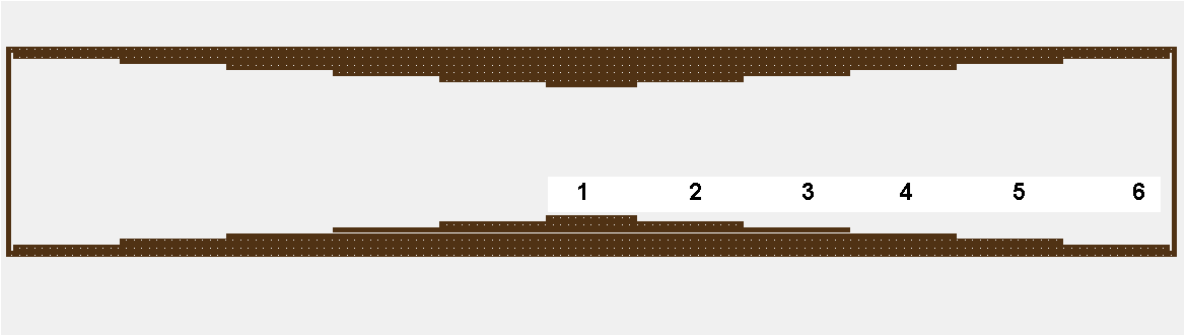

Figure 15: Cross section of the detector device viewed from the front with six pairs of electrodes inside the box.

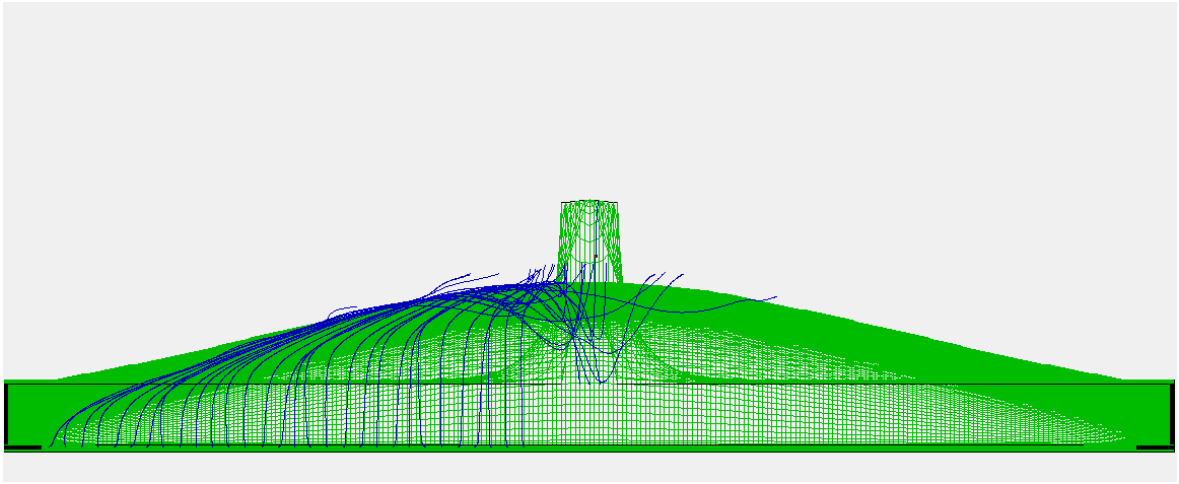

Figure 16: Potential energy (green) and electron trajectories (blue) of the electrodes and the CEM.

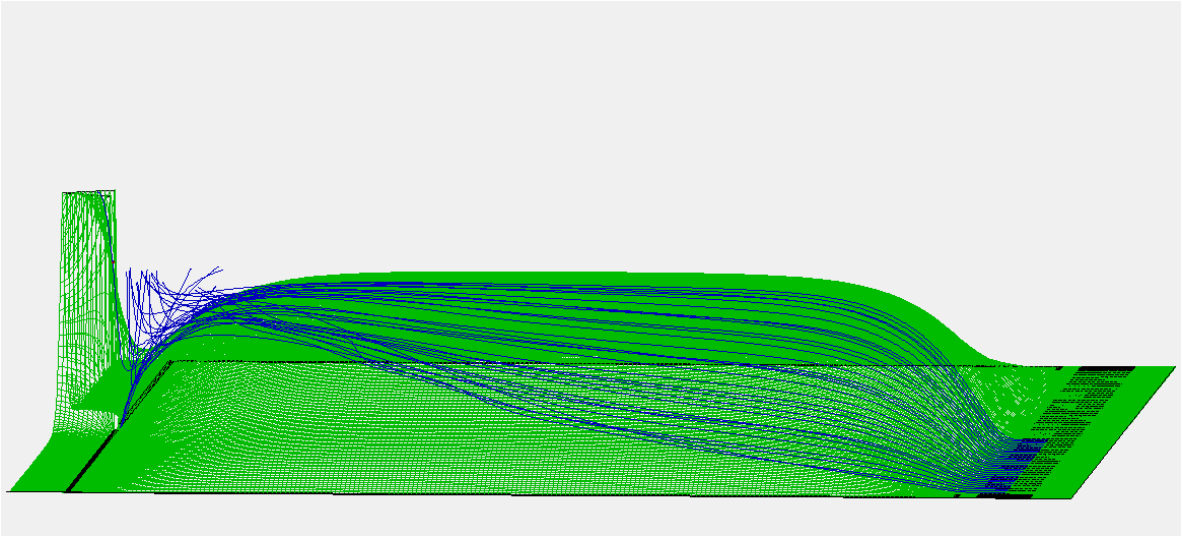

Figure 17: Potential energy (green) and electron trajectories (blue) viewed from the side.

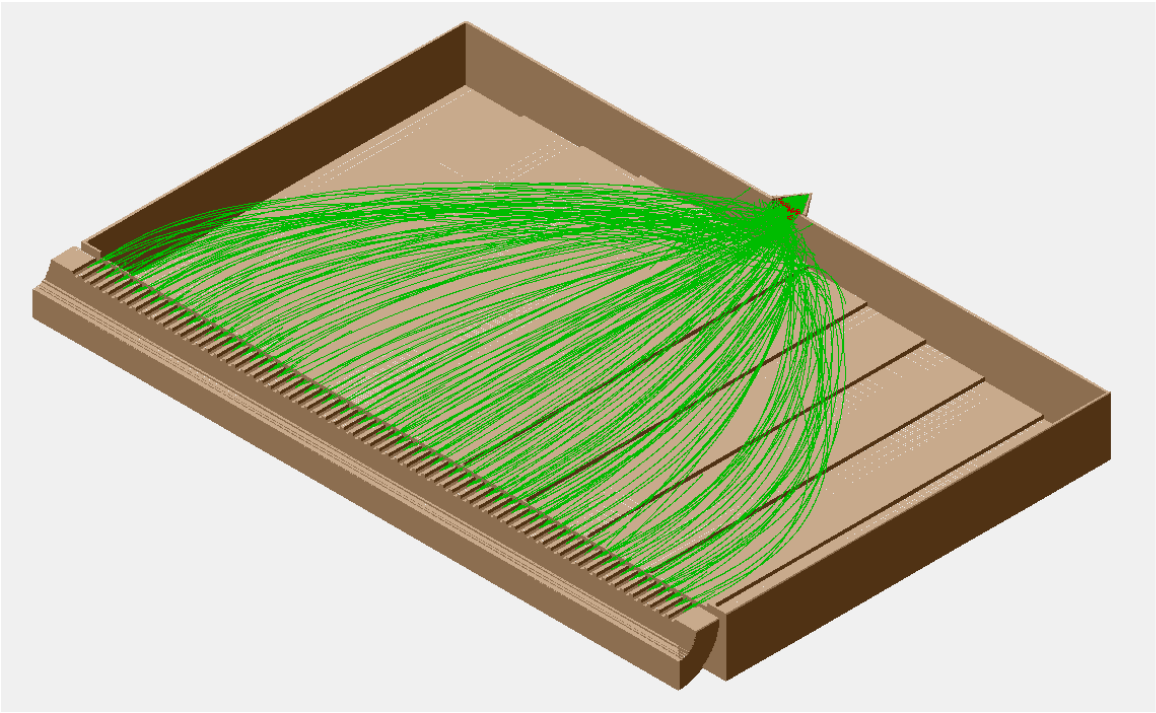

Figure 18: Cross section of the modified detector construction with 400 electrons.

5.3 Transmission Ratio through the Graphite Tube

The transmission of the electrons from the merged laser and ion beam through one aperture of the graphite tube is shown in figure 19 where an imaginary plane, defined at the outer diameter, is recording the coordinates of the electrons transmitted through the aperture. One millimeter is defined as sixteen pixels in the workbench and this allows a more accurate calculations of the electron trajectories.

A sphere distribution with diameter 3 mm, that is equal to the diameter of the laser beam, is placed at the central axis of the of the tube and in front of the aperture. The transmission rate of 65 000 electrons flying in the model is equal to approximately 0.2 %.

A simple model of the transmission as the ratio of the area of a disc, and the area of a sphere, gives the transmission of a source where all the charged particles are directed radially outwards from a single point.

$$\text{Transmission rate (Simple model)} = \frac{2\pi r^2}{4\pi R^2}$$

With r=1.25 mm and R=16 mm, the transmission rate from a point source is equal to approximately 0.3 %. The transmission from the simulation consider charged particles distributed on and inside a sphere at random angle of direction. The deviation from the point source gives a higher probability that the charged particles will collide with the interior of the graphite tube and therefore giving a lower transmission rate.

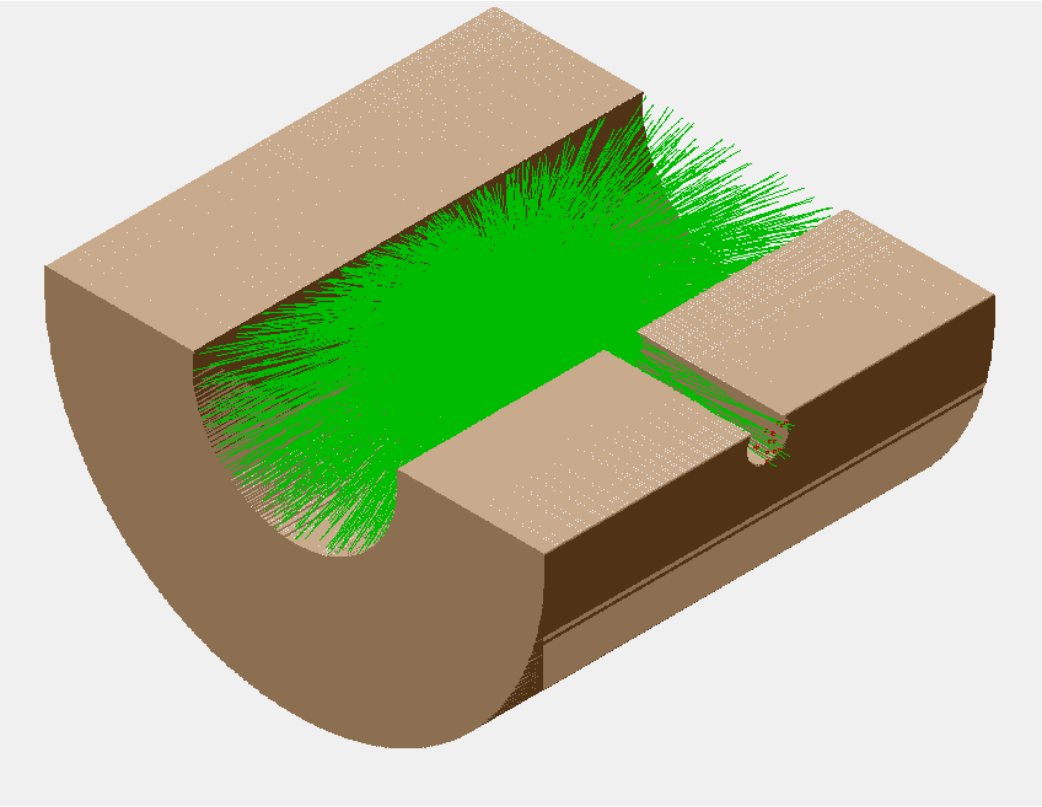

Figure 19: Partition of the graphite tube with one aperture.

5.4 Energy Analyzer

A ninety degree energy analyzer mounted in front of the apertures of the graphite tube deflects and selects a beam with a certain energy through a slit. The magnetic field of the earth can cause the electrons to spin around in a circular path inside the analyzer and to prevent such distortion in the analyzer an acceleration system is modeled between the graphite tube and the cylindrical electrodes of the analyzer. A partition of the graphite tube with accelerator system and energy analyzer is shown in figure 20.

A beam with a certain initial energy in the analyzer, depending on the voltages applied to the accelerating system and the energy of the beam source, is deflected between the cylindrical electrodes and passing through the rectangular aperture of the slit as shown in figure 21. The energy of the green beam in figure 21 is equal to 1 eV and for beam energy that is strictly less than 1 eV the trajectory of the beam deviates from the center position of the aperture and hits the slit to the left of the aperture and if the beam energy is strictly bigger than 1 eV the beam is blocked by the slit to the right of the aperture as the red beam in the figure.

Increasing the kinetic beam energy T to 40 eV and using the scaling rule $T/e\Delta V = constant$ for the setting of the electrodes gives an identical deflection of the beam as in the case with beam energy set to 1 eV.

The resolution of the analyzer is calculated as the ratio of the difference in beam energy ΔE, for which the beam is totally blocked in the device, and the beam energy E, for which all the particles can pass through the aperture of the slit

$$\left|\frac{\Delta E}{E}\right| = \text{resolution}$$

As an example; for the beam energy E =40 eV that can go through the analyzer, the entire beam is totally blocked by the slit for an increased (decreased) energy to 42.3 eV (37,7 eV), and gives the energy difference $\Delta E = \pm$ 2.3 eV. The resolution is equal to

$$\left|\frac{\Delta E}{E}\right| = \frac{2.3}{40} = 0.0575$$

or a 5.75 % deviation from the beam energy E =40 eV blocks the entire signal.[3]

Table 4 shows the resolution of the analyzer for the beam energies in the range 1-40 eV with scaled voltage settings of the electrodes according to the scaling rule (higher beam energies gives smaller rounding errors in the calculations of the resolution).

A higher resolution of the analyzer can be achieved by setting the electrodes in the accelerating system to merely 0.7 volts instead of 10 volts causing the beam to be thicker inside the analyzer but having a more narrow part as shown in figure 22. Also the aperture should be more narrow when the beam can be more focused for gaining higher resolution.

The purpose of the acceleration system is delimited at low voltage settings and distortions in signal can occur. A solution is, instead of using an accelerator system, a shielding of the analyzer, or the whole angular resolution detector, in a μ-metal[4] box preventing the outer magnetic field to interact with the electrons from the beam.

[3]A resolution of 5-6 % is rather low. At energies 40 eV a satisfactory resolution would be 1.25 % where deviations of 40$\pm$0.5 eV could be distinguished.

[4]A μ-metal has a high magnetic susceptibility.

Table 4: Resolution of the energy analyzer for the beam energies in the range 1-40 eV.

Beam energy, eV	Resolution, %
1	7.00
10	6.30
20	6.25
30	6.13
40	5.75

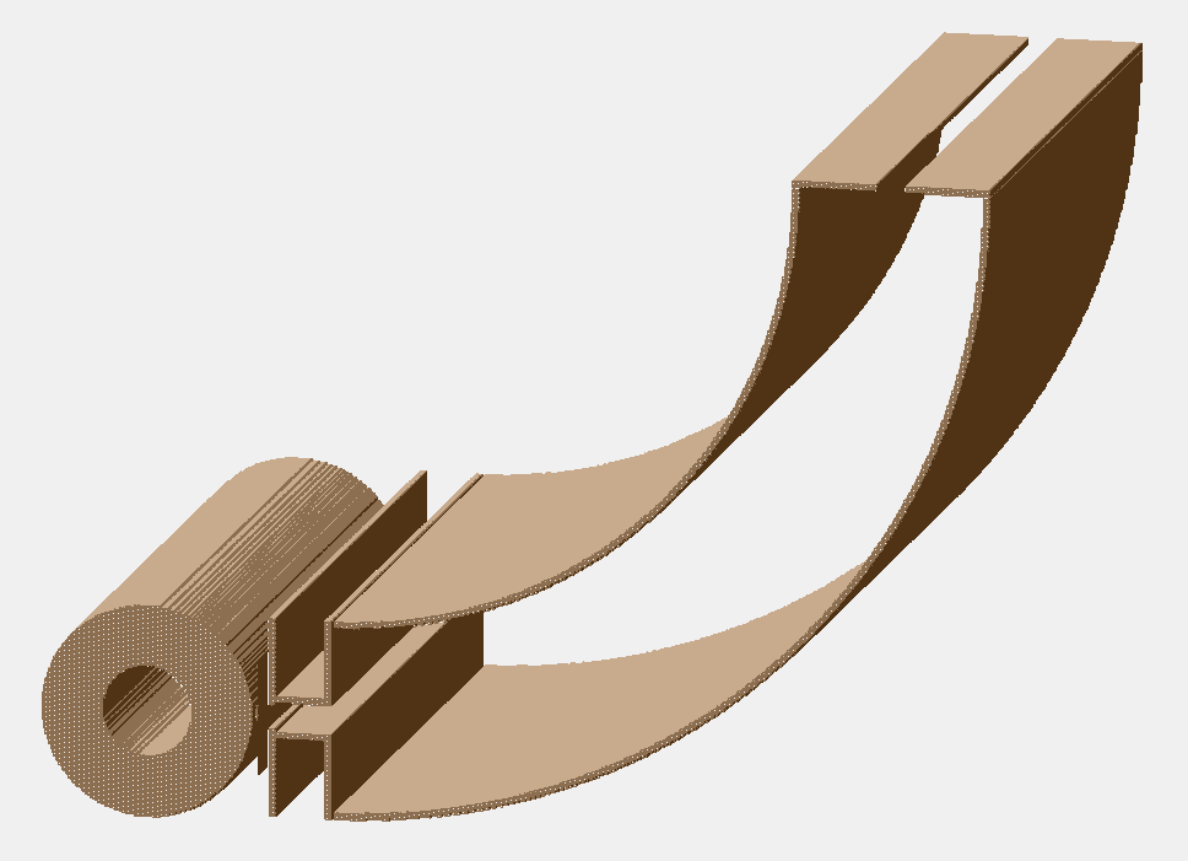

Figure 20: Energy analyzer and graphite tube.

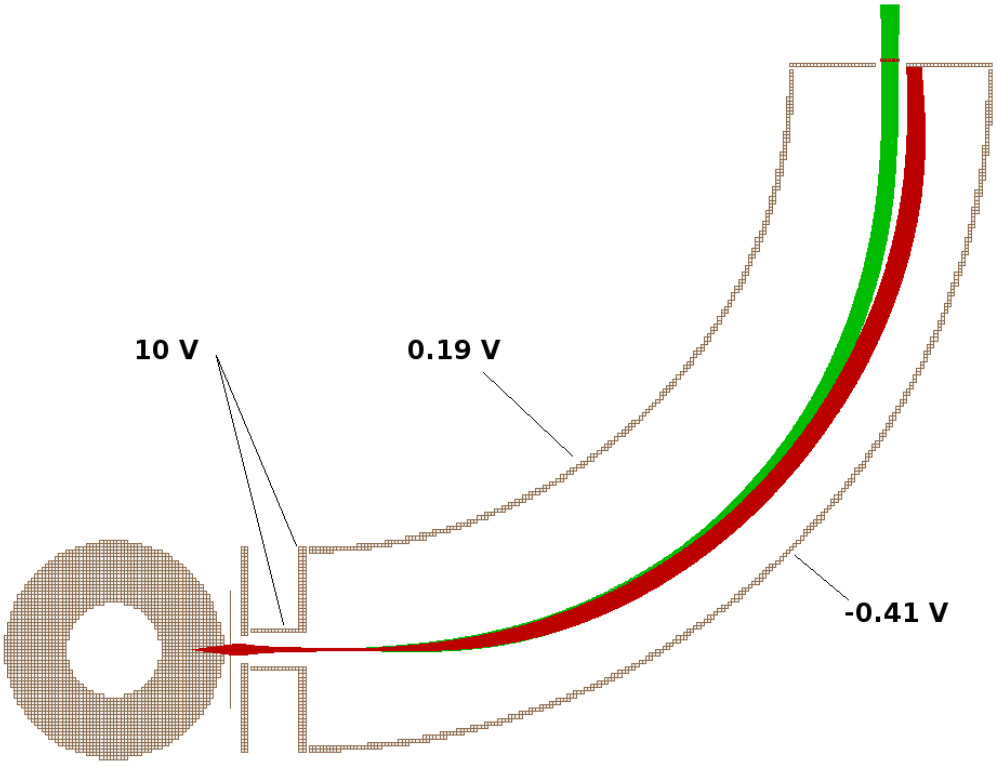

Figure 21: Energy analyzer and graphite tube with two ion beams.

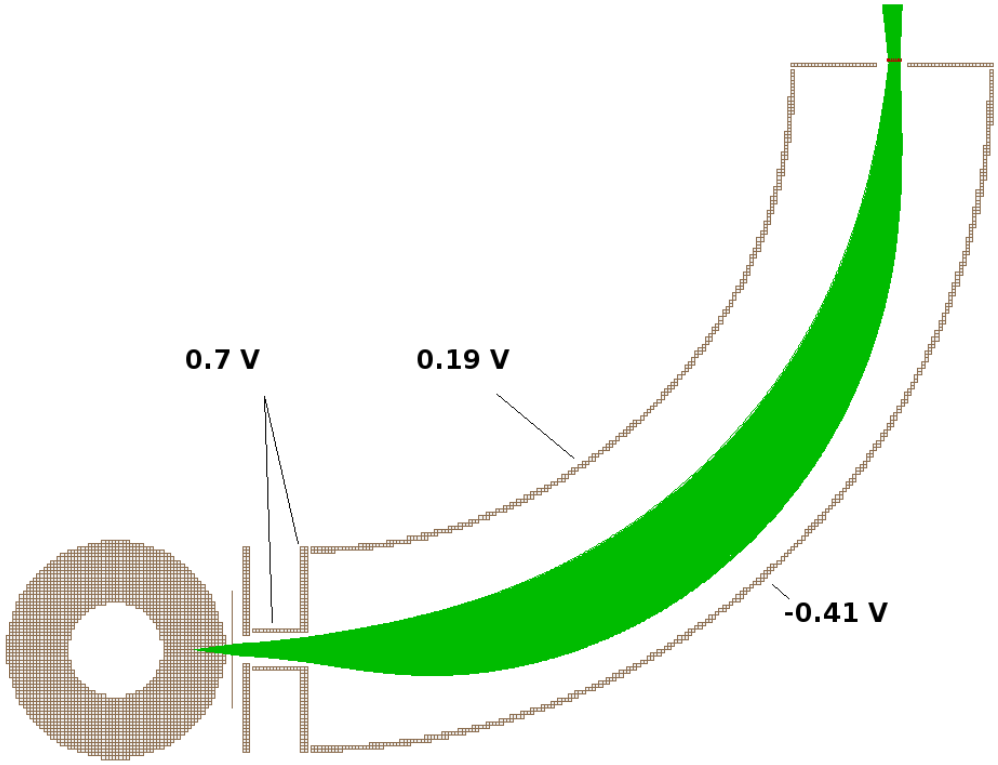

Figure 22: Energy analyzer with low acceleration of the beam.

An observation of figure 21 shows that from the narrow source a relatively wide beam is formed at the aperture of the slit and to get a higher resolution we examine the equations of motion inside the analyzer and how the initial conditions of the beam at the entrance can give a focused point at the exit.

The radial electrical field E of the energy analyzer in figure 23 below is given by

$$E = \frac{E_0 R}{r}$$

and

$$E_0 = -\frac{2T_0}{eR},$$

where E_0 is the field on the central path R with the kinetic energy T_0. The potential is zero on R and outside the cylindrical electrodes.

With the coordinates (y, z)=(r-R, z_1+Rφ) the equations of motions are

$$\ddot{r} = r\dot{\varphi}^2 + \frac{e}{m}E$$

$$r^2\dot{\varphi} = constant$$

and introducing ω as the value of $\dot{\varphi}$ for the central path gives the equation

$$\ddot{y} = -2\omega^2 y$$

the deviation y from the central path R is proportional to

$$y \propto \sin(\sqrt{2}\omega t) = \sin(\sqrt{2}\varphi)$$

A Φ=90 degree analyzer with a point source at z_1 gives an unfocused point at z_2 since, with $\varphi = \pi/2$, $y \propto \sin(\sqrt{2}\pi/2) \neq 0$. The position of the image Q from the source P is given by

$$\varphi_Q - \varphi_P = \frac{\pi}{\sqrt{2}} = 127.2 \text{ degrees}$$

An analyzer with a deflection of Φ=127.2 degrees and with a point source at z_1 gives a point of focus at z_2 allowing a slit with a narrow aperture that gives a high resolution $E/\Delta E$. A derivation of the equation of motion can be found in [8].

For an analyzer with a first-order focusing there is a formula for the applied voltages on the outer and inner electrodes

$$V_{outer} = V\left(1 - 2\ln\frac{R_2}{R_0}\right)$$

and

$$V_{inner} = V\left(1 - 2\ln\frac{R_1}{R_0}\right)$$

where R_0, R_1 and R_2 is the central path, inner and outer radii, respectively, of the analyzer with the energy V on the charged particles [9].

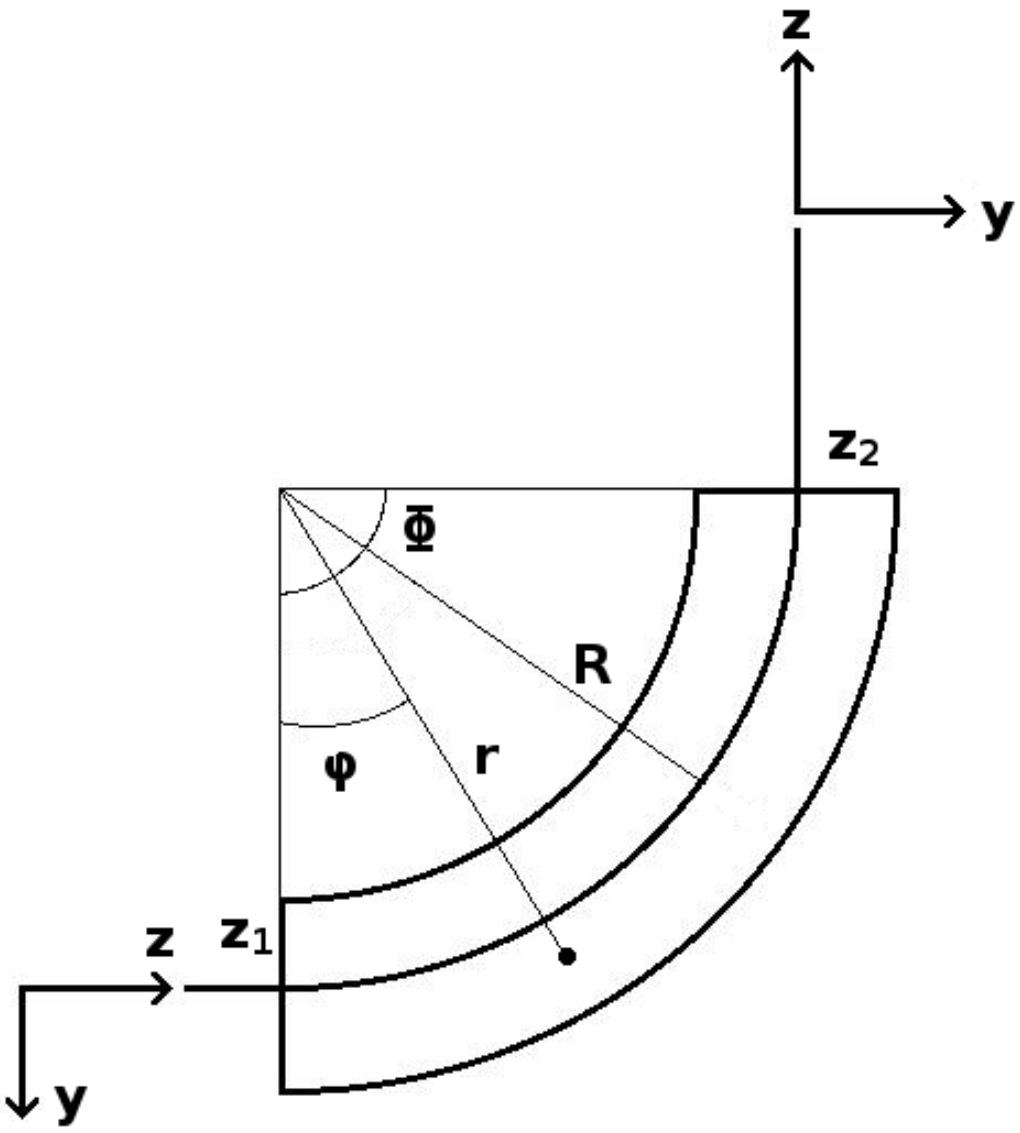

Figure 23: Energy analyzer and coordinates of the path.

5.5 New Version of the Angular Distribution Detector

The laser light has a polarization and the angular distribution of the emitted electrons from the ion beam is measured by rotating the polarization. The highest and lowest intensity of the electron transmission occurs when polarization is in vertical direction relative to the central axis of the graphite tube and at polarization directed at the apertures, respectively. The differential cross section for the emitted electrons from the merging beams is given by

$$\frac{d\sigma}{d\Omega} = \frac{\sigma}{4\pi}[1 + \beta P_2(\cos\theta)] \tag{6}$$

where the total cross section

$$\sigma = \frac{(\text{number of photodetached ions})}{(\text{number of ions})(\text{number of photons})}\frac{1}{\Delta t}$$

gives the photoelectron yield, β is the asymmetry parameter that determines the angular distribution, and $P_2(\cos\theta) = (3\cos^2\theta - 1)/2$ is the Legendre polynomial of the second order with θ as the angle between the emitted electron and the polarization vector of the laser light.

The angular distribution of electrons is obtained by measuring the electron current as a function of the angle of the polarization of the laser beam. By measuring the photoelectron yield with a CEM, as the polarization is rotated from 0° to 180°, gives a value for β as a function of photoelectron energy [10].

The electron distribution is proportional to $\sin^2\theta$ ($\cos^2\theta$), for $\beta = -1$ (2) and the electrons are emitted in a uniform direction, that is an isotropic distribution, when $\beta = 0$.

The experiment is performed in the laboratory (lab) frame and the physical information is in the center-of-mass(CM) frame.

Electrons that are collected in the CEM perpendicular to the ion beam are ejected backwards in the CM-frame with velocity equal to the ion beam. The angles between the velocities in the lab and the CM frame and the vector of the polarization p of the laser light is shown in figure 24; electrons along the x-axis with velocity v_{lab} is traveling backwards in the CM frame with velocity v_{cm} when emitted from the ion beam.

The angle θ_{cm} between the electrons and the laser polarization p in the CM-frame is equal to

$$\cos(\theta_{cm}) = \cos(\alpha)\cos(\theta_{lab}) \tag{7}$$

and

$$\sin(\alpha) = \frac{|v_{ions}|}{|v_{cm}|}$$

where v_{ions} is the velocity of the ions in the beam inside the graphite tube and v_{cm} is the velocity of the electrons. It is not possible to detect electrons when $|v_{cm}| < |v_{ions}|$.

If the laser is polarized along the z-axis then $\theta_{lab} = 90°$, and equation (7) gives $\theta_{cm} = 90°$, all the electrons are emitted perpendicular to the polarization.

Calculating the beam intensity I for $\theta_{cm} = 0^\circ$ gives a value of the parameter β. From (6) and the Legendre polynomial the angular distribution is expressed as

$$I_{cm}(\theta_{cm}) = I_{cm}(0^\circ) + [1 - I_{cm}(0^\circ)] \sin^2 \theta_{cm}$$

and when $I_{cm}(0^\circ)$ and $I_{cm}(90^\circ)$ are known then we have

$$\frac{I_{cm}(0^\circ)}{I_{cm}(90^\circ)} = \frac{\frac{\sigma}{4\pi}[1 + \beta P_2(\cos 0^\circ)]}{\frac{\sigma}{4\pi}[1 + \beta P_2(\cos 90^\circ)]} = \frac{1+\beta}{1-\beta/2}$$

finally solving for β

$$\boxed{\beta = \frac{2\left(\frac{I_{cm}(0^\circ)}{I_{cm}(90^\circ)}\right) - 2}{\left(\frac{I_{cm}(0^\circ)}{I_{cm}(90^\circ)}\right) + 2}}$$

Detecting electrons in two perpendicular directions simultaneously makes it possible to measure the β parameter without rotating the polarization of the laser. Figure 25 shows a compounded picture of the previous parts from the analyzer simulation with two perpendicular analyzers mounted on the graphite tube. A numerical computational example and further theory can be found in [1].

The asymmetry parameter can also be given by the Cooper-Zare formula for photodetachment of an electron with initial orbital angular momentum l

$$\beta = \frac{l(l-1)R_{l-1}^2 + (l+1)(l+2)R_{l+1}^2 - 6l(l+1)R_{l+1}R_{l-1}\cos(\delta_{l+1} - \delta_{l-1})}{(2l+1)[lR_{l-1}^2 + (l+1)R_{l+1}^2]} \tag{8}$$

where the dipole radial matrix element $R_{l\pm1} \propto k^{l\pm1}$ for the wave number k of the continuum electron.[5] The phase shift between two outgoing waves is given by $\cos(\delta_{l+1} - \delta_{l-1})$.

As an example of calculation for photodetachment of the negative ion of oxygen O^-; the initial orbital angular momentum is equal to $l = 1$, the continuum states are s and d waves and with no phase shift between them gives $\cos(\delta_{l+1} - \delta_{l-1}) = 1$. We have the ratio of the matrix elements $R_2/R_0 \propto k^2$ and for the energy ε of the photoelectron and A_2 as a measure of the size of the negative ion we get the ratio $R_2/R_0 = A_2\varepsilon$. Inserting these values in (8) and with the phase shift 1=c we obtain the parameter

$$\beta = \frac{2A_2\varepsilon(A_2\varepsilon - 2c)}{1 + 2A_2^2\varepsilon^2}$$

By measuring the asymmetry parameter from experiments, the size of the negative ion can be obtained. The example above and further theory can be found in [10].

[5] Assuming that there is no interaction between the continuum state electron and the neutral atom.

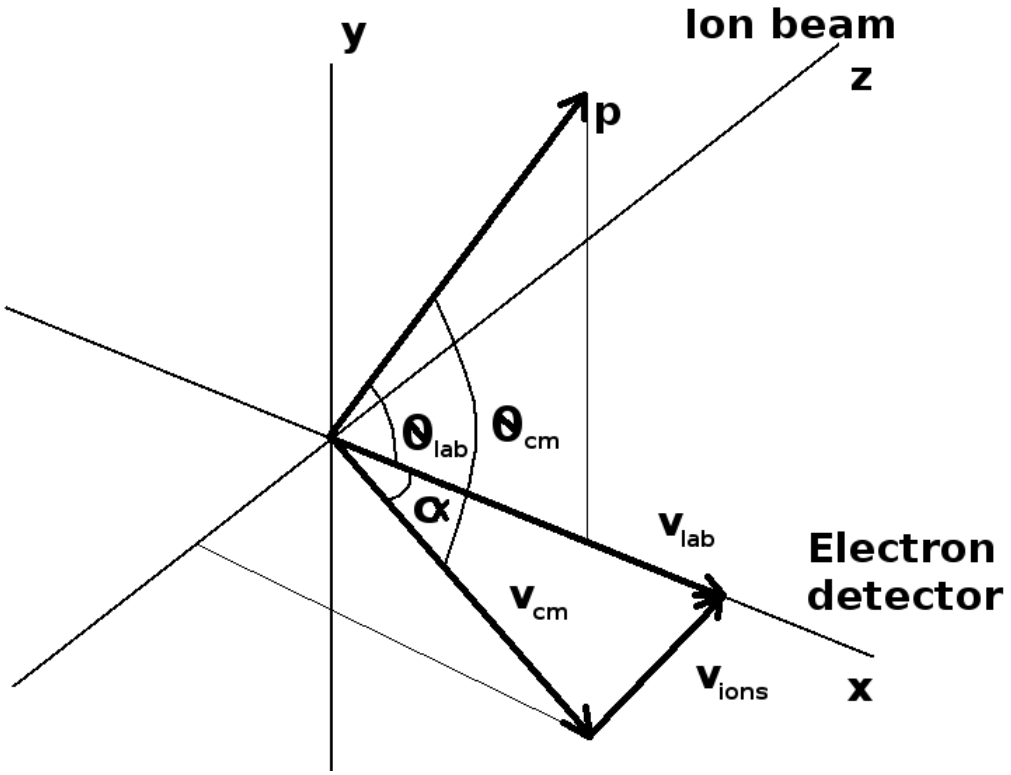

Figure 24: Velocities and polarization vectors with angles in the CM and lab frame.

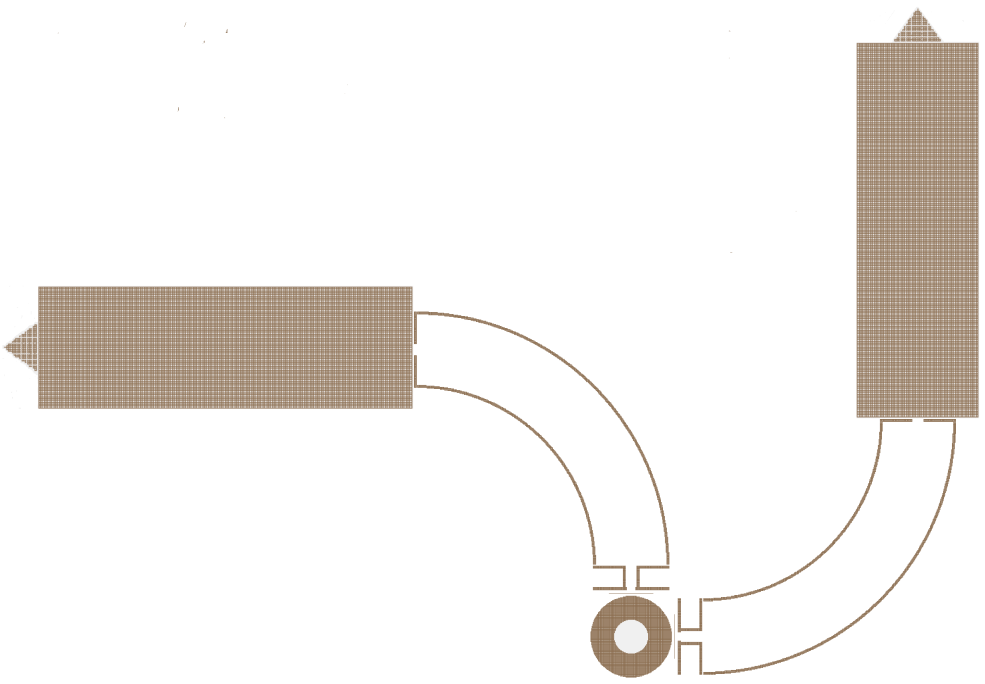

Figure 25: Graphite tube with two setups of energy analyzers.

6 Conclusions and Outlook

The channel electron multiplier (CEM) in the angular resolution electron detector device is attracting a rather low ratio of the electrons emitted from the merged ion and laser beam aligned along the central axis inside the graphite tube. In the range of 200-800 volts applied to the CEM the transmission rate is of the order $\simeq$ 21-31 % (table 1, page 25) for the fixed beam energy of 1 eV.

In a modified model, with six pairs of electrodes added inside the box between the source of the emitted electrons and the CEM, the transmission rate increases a nearly threefold of order for the same range of voltages applied and beam energy; $\simeq$ 60-86 % (table 2, page 30). An increased transmission rate of electrons in the detector makes it faster to collect data and therefore makes it possible to perform experiments.

Further simulations with different initial beam energies in the modified version of the angular resolution electron detector device needs to be done. The transmission rate is decreasing (table 3, page 30) when using a scaling rule, $T/e\Delta V$ =constant, for different beam energies and scaled voltage settings to the combined electrodes inside the box. Optimization of electrode settings for various beam energies needs to be determined in order to use the modified detector in experiments.

Acknowledgments

I would like to give many thanks to professor Dag Hanstorp for supervising me in this project.

References

[1] Dag Hanstorp *An ion beam apparatus for collinear photodetachment experiments* Nuclear Instruments and Methods in Physics Research B (1995) 165-175

[2] C. Diehl, K. Wendt, A. O. Lindahl, P. Andersson, and D. Hanstorp *Ion optical design of a collinear laser-negative ion beam apparatus* Review of Scientific Instruments 82, 053302 (2011)

[3] T. Andersen, H. K. Haugen, H. Hotop *Binding Energies in Atomic Negative Ions: III* J. Phys. Chem. Ref. Data, Vol. 28, No. 6, 1999

[4] David J Manura, David A. Dahl *SIMION Version 8.0 User Manual* Scientific Instrument Services, Inc. (SIMION 8, 2006-2008) Idaho National Laboratory (SIMION 7, 2000)

[5] David J. Griffiths *Introduction to Electrodynamics* Pearson Education, Inc., 2008

[6] Michael T. Heath *Scientific Computing-An Introductory Survey* McGraw-Hill 2002

[7] Autar Kaw, Egwu Kalu *Numerical Methods with Applications* autarkaw.com 2008

[8] Poul Dahl *Introduction to Electron and Ion Optics* Academic Press, Inc., 1973

[9] John H. Moore, Christopher C. Davis, Michael A. Coplan *Building Scientific Apparatus* Perseus Books 2003

[10] D. Hanstorp, C. Bengtsson, D. J. Larson *Angular distribution in photodetachment of O^-* Physical Review A, Vol. 40, No. 2, 1989

A

The program code for creating the geometry of the modified model examined in section 5.2 is given below and 4 graphical units (gu) in the workbench is defined as 1 mm. Scaling the units with 1/4=0.25 in SIMION transform the measure from graphical units to millimeter in the workbench.

```
;1mm=4gu (scale=0.25 in SIMION)

pa_define(708,179,1001,p,n) ;Define a 3d-array to
                            ;contain the device geometry.

locate(0,89,500)     ;center object in cylinder volume
{

locate(0,0,0,1)
      {
      fill                        ;Volume fill.
            {
             within               ;Include volume.
                  {
                   circle(0,0,64) ;Tube with radius 16mm=64gu
                                  ;with infinite z extent.
                   }

                   notin{cylinder(0,0,500,26,26,1000)}

                  ;Makes a circular hole with radius
                  ;6.5mm=26gu in the circular rod.



locate(0,0,-462,1,-90)        ;Hole no. 1.
{
notin{cylinder(0,0,0,4,4,64)}
  ;Makes a small hole in the side of the circular rod.

}
locate(0,0,-448,1,-90)        ;Hole no. 2.
{
notin{cylinder(0,0,0,4,4,64)}
}
locate(0,0,-434,1,-90)        ;Hole no. 3.
{
notin{cylinder(0,0,0,4,4,64)}
}
```

```
locate(0,0,-420,1,-90)        ;Hole no. 4.
{
notin{cylinder(0,0,0,4,4,64)}
}
locate(0,0,-406,1,-90)        ;Hole no. 5.
{
notin{cylinder(0,0,0,4,4,64)}
}
locate(0,0,-392,1,-90)        ;Hole no. 6.
{
notin{cylinder(0,0,0,4,4,64)}
}
locate(0,0,-378,1,-90)        ;Hole no. 7.
{
notin{cylinder(0,0,0,4,4,64)}
}
locate(0,0,-364,1,-90)        ;Hole no. 8.
{
notin{cylinder(0,0,0,4,4,64)}
}
locate(0,0,-350,1,-90)        ;Hole no. 9.
{
notin{cylinder(0,0,0,4,4,64)}
}
locate(0,0,-336,1,-90)        ;Hole no. 10.
{
notin{cylinder(0,0,0,4,4,64)}
}
locate(0,0,-322,1,-90)        ;Hole no. 11.
{
notin{cylinder(0,0,0,4,4,64)}
}
locate(0,0,-308,1,-90)        ;Hole no. 12.
{
notin{cylinder(0,0,0,4,4,64)}
}
locate(0,0,-294,1,-90)        ;Hole no. 13.
{
notin{cylinder(0,0,0,4,4,64)}
}
locate(0,0,-280,1,-90)        ;Hole no. 14.
{
notin{cylinder(0,0,0,4,4,64)}
}
locate(0,0,-266,1,-90)        ;Hole no. 15.
{
```

```
notin{cylinder(0,0,0,4,4,64)}
}
locate(0,0,-252,1,-90)        ;Hole no. 16.
{
notin{cylinder(0,0,0,4,4,64)}
}
locate(0,0,-238,1,-90)        ;Hole no. 17.
{
notin{cylinder(0,0,0,4,4,64)}
}
locate(0,0,-224,1,-90)        ;Hole no. 18.
{
notin{cylinder(0,0,0,4,4,64)}
}
locate(0,0,-210,1,-90)        ;Hole no. 19.
{
notin{cylinder(0,0,0,4,4,64)}
}
locate(0,0,-196,1,-90)        ;Hole no. 20.
{
notin{cylinder(0,0,0,4,4,64)}
}
locate(0,0,-182,1,-90)        ;Hole no. 21.
{
notin{cylinder(0,0,0,4,4,64)}
}
locate(0,0,-168,1,-90)        ;Hole no. 22.
{
notin{cylinder(0,0,0,4,4,64)}
}
locate(0,0,-154,1,-90)        ;Hole no. 23.
{
notin{cylinder(0,0,0,4,4,64)}
}
locate(0,0,-140,1,-90)        ;Hole no. 24.
{
notin{cylinder(0,0,0,4,4,64)}
}
locate(0,0,-126,1,-90)        ;Hole no. 25.
{
notin{cylinder(0,0,0,4,4,64)}
}
locate(0,0,-112,1,-90)        ;Hole no. 26.
{
notin{cylinder(0,0,0,4,4,64)}
}
```

```
locate(0,0,-98,1,-90)          ;Hole no. 27.
{
notin{cylinder(0,0,0,4,4,64)}
}
locate(0,0,-84,1,-90)          ;Hole no. 28.
{
notin{cylinder(0,0,0,4,4,64)}
}
locate(0,0,-70,1,-90)          ;Hole no. 29.
{
notin{cylinder(0,0,0,4,4,64)}
}
locate(0,0,-56,1,-90)          ;Hole no. 30.
{
notin{cylinder(0,0,0,4,4,64)}
}
locate(0,0,-42,1,-90)          ;Hole no. 31.
{
notin{cylinder(0,0,0,4,4,64)}
}
locate(0,0,-28,1,-90)          ;Hole no. 32.
{
notin{cylinder(0,0,0,4,4,64)}
}
locate(0,0,-14,1,-90)          ;Hole no. 33.
{
notin{cylinder(0,0,0,4,4,64)}
}
locate(0,0,0,1,-90)            ;CENTER. Hole no. 34
{
notin{cylinder(0,0,0,4,4,64)}
}
locate(0,0,14,1,-90)           ;Hole no. 35.
{
notin{cylinder(0,0,0,4,4,64)}
}
locate(0,0,28,1,-90)           ;Hole no. 36.
{
notin{cylinder(0,0,0,4,4,64)}
}
locate(0,0,42,1,-90)           ;Hole no. 37.
{
notin{cylinder(0,0,0,4,4,64)}
}
locate(0,0,56,1,-90)           ;Hole no. 38.
{
```

```
notin{cylinder(0,0,0,4,4,64)}
}
locate(0,0,70,1,-90)          ;Hole no. 39.
{
notin{cylinder(0,0,0,4,4,64)}
}
locate(0,0,84,1,-90)          ;Hole no. 40.
{
notin{cylinder(0,0,0,4,4,64)}
}
locate(0,0,98,1,-90)          ;Hole no. 41.
{
notin{cylinder(0,0,0,4,4,64)}
}
locate(0,0,112,1,-90)         ;Hole no. 42.
{
notin{cylinder(0,0,0,4,4,64)}
}
locate(0,0,126,1,-90)         ;Hole no. 43.
{
notin{cylinder(0,0,0,4,4,64)}
}
locate(0,0,140,1,-90)         ;Hole no. 44.
{
notin{cylinder(0,0,0,4,4,64)}
}
locate(0,0,154,1,-90)         ;Hole no. 45.
{
notin{cylinder(0,0,0,4,4,64)}
}
locate(0,0,168,1,-90)         ;Hole no. 46.
{
notin{cylinder(0,0,0,4,4,64)}
}
locate(0,0,182,1,-90)         ;Hole no. 47.
{
notin{cylinder(0,0,0,4,4,64)}
}
locate(0,0,196,1,-90)         ;Hole no. 48.
{
notin{cylinder(0,0,0,4,4,64)}
}
locate(0,0,210,1,-90)         ;Hole no. 49.
{
notin{cylinder(0,0,0,4,4,64)}
}
```

```
locate(0,0,224,1,-90)          ;Hole no. 50.
{
notin{cylinder(0,0,0,4,4,64)}
}
locate(0,0,238,1,-90)          ;Hole no. 51.
{
notin{cylinder(0,0,0,4,4,64)}
}
locate(0,0,252,1,-90)          ;Hole no. 52.
{
notin{cylinder(0,0,0,4,4,64)}
}
locate(0,0,266,1,-90)          ;Hole no. 53.
{
notin{cylinder(0,0,0,4,4,64)}
}
locate(0,0,280,1,-90)          ;Hole no. 54.
{
notin{cylinder(0,0,0,4,4,64)}
}
locate(0,0,294,1,-90)          ;Hole no. 55.
{
notin{cylinder(0,0,0,4,4,64)}
}
locate(0,0,308,1,-90)          ;Hole no. 56.
{
notin{cylinder(0,0,0,4,4,64)}
}
locate(0,0,322,1,-90)          ;Hole no. 57.
{
notin{cylinder(0,0,0,4,4,64)}
}
locate(0,0,336,1,-90)          ;Hole no. 58.
{
notin{cylinder(0,0,0,4,4,64)}
}
locate(0,0,350,1,-90)          ;Hole no. 59.
{
notin{cylinder(0,0,0,4,4,64)}
}
locate(0,0,364,1,-90)          ;Hole no. 60.
{
notin{cylinder(0,0,0,4,4,64)}
}
locate(0,0,378,1,-90)          ;Hole no. 61.
{
```

```
notin{cylinder(0,0,0,4,4,64)}
}
locate(0,0,392,1,-90)         ;Hole no. 62.
{
notin{cylinder(0,0,0,4,4,64)}
}
locate(0,0,406,1,-90)         ;Hole no. 63.
{
notin{cylinder(0,0,0,4,4,64)}
}
locate(0,0,420,1,-90)         ;Hole no. 64.
{
notin{cylinder(0,0,0,4,4,64)}
}
locate(0,0,434,1,-90)         ;Hole no. 65.
{
notin{cylinder(0,0,0,4,4,64)}
}
locate(0,0,448,1,-90)         ;Hole no. 66.
{
notin{cylinder(0,0,0,4,4,64)}
}
locate(0,0,462,1,-90)         ;Hole no. 67.
{
notin{cylinder(0,0,0,4,4,64)}
}



within                                          ;Include volume.
{
       centered_box3d(68,0,0,0.5,70,984)        ;Mesh.
}

within
{
       centered_box3d(372,0,0,596,178,1000)
         ;Box. Outer surface.
}

       notin{centered_box3d(372,0,0,586,168,990)}
        ;Box. Cavity.

       notin{centered_box3d(76,0,0,4,12,940)}
        ;Makes a rectangular aperture in the shielding.
```

```
locate(666,0,0,1,-90) ;Locates to the side of the box.
{
       notin{cylinder(0,0,0,20,20,4)}
       ;Makes a hole with a diameter 1cm=40gu in the box
       ;for the detector.
}


}
}


electrode(1) {          ;1st pair of electrodes (closest to the CEM).

fill {
locate(372,57,0)
{
     within {centered_box3d(0,0,0,582,4,78)}
}
locate(372,-57,0)
{
     within {centered_box3d(0,0,0,582,4,78)}
}
}
}



electrode(2) {           ;2nd pair of electrodes.

fill {
locate(372,62,0)
{
     within {centered_box3d(0,0,0,582,4,260)}
}
locate(372,-62,0)
{
     within {centered_box3d(0,0,0,582,4,260)}
}
}
}


electrode(3) {           ;3rd pair of electrodes.

fill {
```

```
locate(372,67,0)
{
     within {centered_box3d(0,0,0,582,4,442)}
}
locate(372,-67,0)
{
     within {centered_box3d(0,0,0,582,4,442)}
}
}
}


electrode(4) {            ;4th pair of electrodes.

fill {
locate(372,72,0)
{
     within {centered_box3d(0,0,0,582,4,624)}
}
locate(372,-72,0)
{
     within {centered_box3d(0,0,0,582,4,624)}
}
}
}


electrode(5) {            ;5th pair of electrodes.

fill {
locate(372,77,0)
{
     within {centered_box3d(0,0,0,582,4,806)}
}
locate(372,-77,0)
{
     within {centered_box3d(0,0,0,582,4,806)}
}
}
}

electrode(6) {            ;6th pair of electrodes.

fill {
locate(372,82,0)
{
```

```
     within {centered_box3d(0,0,0,582,4,988)}
}
locate(372,-82,0)
{
     within {centered_box3d(0,0,0,582,4,988)}
}
}
}
```

```
electrode(7) {              ;Defines the CEM

locate(671,0,0) {           ;Translate position of cone (x,y,z)

     rotate_fill(360) {     ; Degrees around x axis.
         within {
     polyline( 0,0,     ;(x,y) vertex of the triangle of the cone.

               0,26,    ;Radius of the cone.
               36,0)   ;Length if the cone
                  }
           notin{
      polyline(0,0
                  0,20  ;Inner radius of the cone.
                  30,0) ;Inner length of the cone
                 }
                      }
                  }

              }
}
```